

NASA Contractor Report 178105

ICASE REPORT NO. 86-28

NASA-CR-178105
19860017518

ICASE

A SPECTRAL MULTIDOMAIN METHOD FOR THE SOLUTION
OF HYPERBOLIC SYSTEMS

David Kopriva

Contract Nos. NAS1-17070, NAS1-18107
May 1986

INSTITUTE FOR COMPUTER APPLICATIONS IN SCIENCE AND ENGINEERING
NASA Langley Research Center, Hampton, Virginia 23665

Operated by the Universities Space Research Association

LIBRARY COPY

JUN 20 1986

LANGLEY RESEARCH CENTER
LIBRARY, NASA
HAMPTON, VIRGINIA

NASA

National Aeronautics and
Space Administration

Langley Research Center
Hampton, Virginia 23665

A SPECTRAL MULTIDOMAIN METHOD
FOR THE SOLUTION OF HYPERBOLIC SYSTEMS

David A. Kopriva
Florida State University
and
Institute for Computer Applications in Science and Engineering

Dedicated to Milton E. Rose
on Occasion of his 60th Birthday

ABSTRACT

A multidomain Chebyshev spectral collocation method for solving hyperbolic partial differential equations has been developed. Though spectral methods are global methods, an attractive idea is to break a computational domain into several subdomains, and a way to handle the interfaces is described. The multidomain approach offers advantages over the use of a single Chebyshev grid. It allows complex geometries to be covered, and local refinement can be used to resolve important features. For steady-state problems it reduces the stiffness associated with the use of explicit time integration as a relaxation scheme. Furthermore, the proposed method remains spectrally accurate. Results showing performance of the method on one-dimensional linear models and one- and two-dimensional nonlinear gas-dynamics problems are presented.

Research was supported by the National Aeronautics and Space Administration under NASA Contract Nos. NAS1-17070 and NAS1-18107 while the author was in residence at ICASE, NASA Langley Research Center, Hampton, VA 23665-5225.

1. INTRODUCTION

In this paper we address the problem of efficiently computing Chebyshev spectral collocation approximations to quasilinear hyperbolic systems of the form

$$Q_t + A(Q)Q_x + B(Q)Q_y = 0 \quad x,y \in D \subset \mathbb{R}^2, \quad t \geq 0 \quad (1)$$

with appropriate boundary and initial conditions. Here, Q is an m -vector and A and B are $m \times m$ matrices. This system is hyperbolic if for any constants k_1 and k_2 the matrix $T = k_1 A + k_2 B$ has only real eigenvalues and there exists a similarity transformation matrix, P , such that $PTP^{-1} = \Lambda$ is a real diagonal matrix.

In particular, we are interested in the solution of the Euler equations of gas dynamics which form a system of this type. The use of the nonconservation form is justified for problems in which shocks are fitted and in this situation spectral methods work well [1]. Problems of the type presented in Ref. [1] provide the motivation for what follows.

The typical Chebyshev spectral collocation procedure for the solution of the system (1) is described in several reviews such as those of Gottlieb, Hussaini, and Orszag [2], and Hussaini, Salas, and Zang [3]. First, the domain of interest is mapped onto the square $D' = [-1,1] \times [-1,1]$ and an $(N+M) \times (M+1)$ point mesh is generated with the collocation points defined by

$$\begin{aligned} x_i &= -\cos(i\pi/N) & i &= 0, 1, \dots, N \\ y_j &= -\cos(j\pi/M) & j &= 0, 1, \dots, M. \end{aligned} \quad (2)$$

Mesh point values of Q , designated by Q_{ij} , are associated with each of the collocation points (x_i, y_j) . A global Chebyshev interpolant of order N in the x direction and order M in the y direction is then put through the mesh point values

$$Q_p(x, y) = \sum_{n,m=0}^{N,M} a_{nm} T_n(x) T_m(y). \quad (3)$$

Approximations to the derivatives at the collocation points are computed by differentiating the interpolant and evaluating the resulting polynomial at the collocation points. The computation of the derivatives can be accomplished in one of two ways (see Gottlieb, et al., [2]): The first is to take advantage of the fact that the sums for both the interpolant and its derivative reduce to cosine sums at the chosen collocation points. For example

$$\frac{dQ}{dx} = \sum_{n,m=0}^{N,M} a_{nm} T'_n(x) T_m(y) = \sum_{n,m=0}^{N,M} b_{nm} T_n(x) T_m(y) \quad (4)$$

where

$$b_{Nm} = 0,$$

$$b_{N-1,m} = 2Na_{nm} \quad (5)$$

and

$$c_n b_{nm} = b_{n+2,m} + 2(n+1)a_{n+1,m} \quad \text{for } 0 \leq n \leq N-2.$$

The constant c_n is defined as $c_n = 2$ for $n = 0, N$ and $c_n = 1$ otherwise. The advantage of this form is that a fast cosine transform can compute the derivatives along each y line in $O(N \log N)$ operations.

The other approach to computing the derivatives is to write the differentiation operation as the product of a differentiation matrix and the a vector of the Q_{1j} 's. For example, along each y line the x derivative is

$$\left(\frac{dQ}{dx}\right)_j = D(Q_p)_j \quad (6)$$

where $(Q_p)_j = [Q_{0,j} \ Q_{1,j} \ \dots \ Q_{N,j}]^T$ and the elements of the matrix D are defined in Gottlieb et al., [2]. The amount of work with this procedure is of $O(N^2)$. What one loses in efficiency one gains as flexibility in the number of mesh points that can be used in each direction without adding storage.

No matter which way the spatial derivatives are computed, it is important to note that computing the Chebyshev derivative approximations requires only mesh point values. Derivatives at the end points require only points interior to the mesh so no extra procedure is required to compute derivatives at boundaries.

Once the spatial derivatives are approximated, what results is a system of ordinary differential equations in time for the variation of the solution at each collocation point (Method of Lines). Because the differentiation matrix is full, explicit methods are typically used to integrate the semi-discrete equations. In this paper, all time integrations will be performed with a fourth-order Runge-Kutta method.

The advantage of using this spectral method to solve (1) is that for solutions which are $C^\infty(D)$, the accuracy is better than any polynomial order (Canuto and Quarteroni, [4]). This is usually called "spectral accuracy" and asymptotic behavior can be observed if there are enough grid points to

adequately resolve the solution. It is thus possible to compute to a given spatial accuracy with fewer grid points than required by typical low-order finite difference approximations.

Balancing the high accuracy of the spectral method, however, are some major disadvantages of the typical Chebyshev collocation approach:

- (1) It may not be easy or even possible to map $D \rightarrow D^*$ globally.
- (2) The collocation point distribution is global and predetermined. Local refinement of the mesh is not possible.
- (3) The points are concentrated near the boundaries where they are typically not needed for hyperbolic problems.
- (4) If explicit time integration is used the time step restriction in one dimension is proportional to $1/N^2$.
- (5) For complete flexibility in the number of mesh points which can be used, the derivatives cost of $O(N^2)$ in each direction.

These problems can be reduced significantly by breaking up the region D into several subdomains D_k each of which has its own Chebyshev grid. With a stable and efficient method for computing the interfaces, the advantages of such an approach would be:

- (1) Complicated geometries can be covered.
- (2) Points can be distributed with some flexibility; local refinement is possible.
- (3) In one dimension, with N points and K subdomains, the time step restriction increases to $\Delta t \propto K/N^2$.
- (4) Derivative evaluation work with matrix multiplication decreases to $K(N/K)^2$ or $1/K$ that of a single grid.

The idea of breaking up the computational domain into subdomains each with a different grid is not new. For finite difference methods this is a currently popular approach (e.g., [5]). For spectral methods, however, previous applications have been limited to elliptic and parabolic problems. Orszag [6] first applied such a technique to solve elliptic problems. He enforced continuity of the function and its first derivative as the interface condition. Metivet and Morchoisne [7] and later, Morchoisne [8] computed multidomain solutions to the Navier-Stokes equations. Recently, Patera [9] and Korczak and Patera [10] have been using a spectral element method to solve the incompressible Navier-Stokes equations. Their method is very similar to the p finite-element methods developed by Babuska (see [10]) but uses Chebyshev interpolants. The treatment of the convective terms, however, does not lend itself to purely convective problems. For these problems, we describe the method below.

2. MULTIDOMAIN APPROACH

In this paper, we will break up the physical domain, D , into K subdomains D_k which do not overlap except for the common boundary points. Figure 1 shows a rectangular two-dimensional example of the situation with four subdomains. Each of the D_k are mapped onto a square $[-1,1] \times [-1,1]$. Spatial approximations at interior points of each subdomain are computed in the usual way. Across an interface, however, there are two values of the normal derivative. For example, at the y coordinate line interface between D_1 and D_2 in Figure 1, derivative approximations are available from the left and from the right. The problem is to choose properly information from

the right and the left to give a stable and consistent approximation to the differential equation at the interface.

Before discussing a multidomain method for the boundary value problem (1), we will first examine the one-dimensional case. In one dimension, we seek interface algorithms of the semidiscrete form

$$\frac{\partial Q^I}{\partial \tau} + A^L \frac{\partial Q^L}{\partial x} + A^R \frac{\partial Q^R}{\partial x} = 0 \quad (7)$$

where Q^I denotes the value of Q at an interface and the derivatives superscripted with L and R denote the two spectral approximations computed in the left and right, respectively. For consistency, we require that

$$A^L + A^R = A \quad (8)$$

and for efficiency we want A^L and A^R to be computed with little more work than is required for the computation of A itself.

To generate the coefficient matrices, consider first the linear scalar hyperbolic equation

$$u_t + \lambda u_x = 0 \quad \lambda > 0. \quad (9)$$

Because the equation is hyperbolic, it is clear that the common interface point should depend only on information propagated from the left. Thus, the approximation should be

$$\frac{\partial u^I}{\partial \tau} + \lambda \frac{\partial u^L}{\partial x} = 0. \quad (10)$$

This is, of course, just upwind differencing at the interface and is equivalent to the way Gottlieb and Orszag [11] handled a tau approximation to equation (9). To simplify the computational logic to include cases where the coefficient, λ , is of either sign, the approximation (10) can be written as

$$\frac{\partial u^I}{\partial t} + 1/2 (\lambda + |\lambda|) \frac{\partial u^L}{\partial x} + 1/2 (\lambda - |\lambda|) \frac{\partial u^R}{\partial x} = 0. \quad (11)$$

If we now consider that this equation is a single component of a diagonalized system, where the diagonal matrix

$$\Lambda = \begin{bmatrix} \lambda_1 & & 0 \\ & \lambda_2 & \\ 0 & & \lambda_n \end{bmatrix} = P^{-1} A P,$$

we can write the system as

$$\frac{\partial Q^I}{\partial t} + 1/2 (A + |A|) \frac{\partial Q^L}{\partial x} + 1/2 (A - |A|) \frac{\partial Q^R}{\partial x} = 0 \quad (12)$$

where $|A| = P|\Lambda|P^{-1}$. Formally, this is nothing more than the method of characteristics in one dimension.

We now propose to avoid the computation of the matrix absolute value by approximating it with a diagonal matrix

$$|A| \approx P\lambda^* I P^{-1} = \lambda^* I \quad (13)$$

where λ^* is chosen to lie between the largest and smallest elements of $|\Lambda|$.

The boundary scheme is now of the form of Eq. (7) with

$$A^L = 1/2 (A + \lambda^* I) \quad A^R = 1/2 (A - \lambda^* I). \quad (14)$$

This choice of coefficient matrices always has proper upwind dominance on all of the characteristic variables, but includes some downwind influence. To see this, re-diagonalize the system (7) and use u as the n^{th} component of the diagonalized system. Then the approximation to the method of characteristics causes the characteristic variables at the interface to be approximated by

$$\frac{\partial u^I}{\partial t} + 1/2 (\lambda_n + \lambda^*) \frac{\partial u^L}{\partial x} + 1/2 (\lambda_n - \lambda^*) \frac{\partial u^R}{\partial x} = 0. \quad (15)$$

In fact, this can be viewed as the purely upwind scheme with an error term: For the $\lambda_n > 0$ case,

$$\frac{\partial u^I}{\partial t} + \lambda_n \frac{\partial u^L}{\partial x} = (\lambda^* - \lambda_n) \left(\frac{\partial u^R}{\partial x} - \frac{\partial u^L}{\partial x} \right). \quad (16)$$

Thus, we have the spectrally accurate upwind approximation with an error term proportional to the difference of the right and left spectral derivatives. If the solution has the necessary smoothness, this difference should also decay spectrally and spectral accuracy of the approximation should be retained.

We will study the stability of the multidomain method with the interface approximation (14) numerically. An analytic study of stability is not possible at this time. Stability theory for Chebyshev approximations to hyperbolic initial-boundary value problems is not advanced enough to analyze an approximation which introduces some downwind influence at the interface.

We consider the two-domain approximation of the scalar equation (9) with the interface approximation (12) with $\lambda = 1$. The line segment $[-2,2]$ is divided equally into two domains of $[-2,0]$ on the left and $[0,2]$ on the right. The semidiscrete approximation can be written as a system of ordinary equations with the two-domain coefficient matrix

$$\begin{bmatrix} D^L & 0 \\ 0 & D^R \end{bmatrix} \quad (17)$$

where D^L and D^R are the single domain differentiation matrices for the left and the right, modified to include the interface approximation. For this system to be time stable, that is, the solution does not grow unboundedly as $t \rightarrow \infty$, the eigenvalues of the coefficient matrix must have negative real parts.

Figure 2 shows how the eigenvalues change as λ^* varies when 6 points are used. The case of $\lambda^* = 0$ corresponds to simple averaging and is clearly not time stable. Choosing $\lambda^* > 0$ large enough moves the eigenvalues into the left half of the complex plane and the resulting approximation is time stable. The case of $\lambda^* = 1$ is the purely upwind case and the eigenvalues decouple into two single-domain patterns. If λ^* is chosen equal to, or larger than, the wave speed, λ_n , the approximation has the effect of adding a purely dissipative term to the equation and two purely real eigenvalues are created. If λ^* is very much larger than λ_n , however, the eigenvalues migrate to the right of the imaginary axis. The range of λ^* 's for which the approximation is stable decreases as the disparity in the number of points

becomes larger; for very stiff systems, it may be necessary to use $|A|$ instead of λ^* at the interface.

It is interesting to note that the reverse situation, where there is more resolution on the upstream side of the interface, does not show this behavior and is stable for all $\lambda^* \geq 0$. For systems, this means that λ^* should be chosen to be only slightly larger than the smallest eigenvalue representing a characteristic moving from the coarse to the fine grid. For systems, this means that λ^* should be chosen to be only slightly larger than the smallest eigenvalue representing a characteristic moving from the coarse to the fine grid. We note, however, that the examples on which the scheme has been tested show that the approximation is robust over a wide range of choices of λ^* .

In two dimensions, the upwind weighted approximation is used in the direction perpendicular to the interface. Returning to Figure 1, along x coordinate lines, the y derivatives are continuous across the interfaces except at corners. At points not on the corners, then, we propose using

$$\frac{\partial Q^I}{\partial t} + A^L \frac{\partial Q^L}{\partial x} + A^R \frac{\partial Q^R}{\partial x} + B \frac{\partial Q^I}{\partial y} = 0 \quad (18)$$

where A^L and A^R are defined as above. Along x coordinate interfaces,

$$\frac{\partial Q^I}{\partial t} + A \frac{\partial Q^I}{\partial x} + B^T \frac{\partial Q^L}{\partial y} + B^B \frac{\partial Q^R}{\partial y} = 0 \quad (19)$$

where $B^T = 1/2 (B + \mu^* I)$ and $B^B = 1/2 (B - \mu^* I)$ and μ^* is an approximation to the eigenvalues of B . At corners, the weighted approximations are used in both directions.

3. NUMERICAL EXAMPLES

Numerical experiments on four model problems in one and two dimensions will be presented. The models include the scalar one-dimensional hyperbolic initial boundary value problem for a travelling Gaussian pulse, a linear system in one dimension, quasi-one-dimensional flow in a converging-diverging nozzle, and the transonic Ringleb problem. The Ringleb flow models the smooth nonlinear transonic flow in a curved duct and has an exact solution to which to compare.

A. Solution of a Linear Scalar Problem

The solution to the linear scalar problem

$$\frac{\partial u}{\partial t} + 2 \frac{\partial u}{\partial x} = 0 \quad x \in [-2, 2], \quad t > 0 \quad (20)$$

$$u(x, 0) = \exp(-(x - x_0)^2 / 0.3) \quad x \in [-2, 2]$$

$$u(-2, t) = \exp(-(x - t - x_0)^2 / 0.3) \quad t > 0$$

can be used to examine the effects of varying λ^* in the spatial approximation described in Eq. (15). The time integration for this and all following examples was a fourth-order Runge-Kutta technique. For this and the next model problem the time step was chosen so that the temporal errors were on the order of 10^{-10} . The main questions to be answered here are the effect of the $\lambda^* \neq 2$ on the accuracy of the solution and if reflections are a problem at the interface. Figure 3 shows the computed (circles) and exact (line) solutions for the pulse after it has propagated through the interface at $x = 0$ for two distributions of the mesh points and $\lambda^* = 6$.

The interface approximation Eq. (15) degrades the accuracy of the solution when compared to the purely characteristic interface, $\lambda^* = 2$, if equal resolution is not provided in each subdomain. In no case, however, is the global L_2 error larger than the global error for the characteristic interface. Furthermore, if λ^* remains fixed and the total number of points is increased, the error decay remains spectral. Figure 4 shows the pointwise errors of the solution to Eq. (20) for the situations represented in Figure 3 as λ^* is increased beyond the characteristic value of 2. The situation is worse when more resolution is used upstream of the interface because the approximation includes more and more downwind influence as λ^* is increased. In a practical computation, the effect of the boundary approximation would not be important if the solution were equally resolved in all subdomains.

Reflections at the interface are not visible in Figure 3 even though there is a factor of two difference in the number of collocation points. Gottlieb and Orszag [11] also noticed this for a tau approximation to the scalar wave equation. This is typical for the spectral approximations; examples with up to a factor of three and four in the ratio of the number of mesh points have not shown spurious reflections off of the interface.

B. A Linear System Example

The accuracy of the interface approximation will now be demonstrated with the 2×2 linear system

$$\begin{bmatrix} u \\ v \end{bmatrix}_t + \begin{bmatrix} 1 & 2 \\ 2 & 1 \end{bmatrix} \begin{bmatrix} u \\ v \end{bmatrix}_x \quad x \in [-2, 2], \quad t > 0. \quad (21)$$

The coefficient matrix has eigenvalues $+3$ and -1 so the system has information which propagates in both directions and with different speeds across the interface at $x = 0$. The initial and boundary conditions were chosen so that the characteristic variables were the Gaussian pulses used in the scalar problem, Eq. (20). The coefficient λ^* for this case was chosen to be the maximum eigenvalue, $\lambda = +3$. Figure 5 shows the results for the two components of this system at a time when the characteristic pulses have crossed the interface. In Figure 5a there are twice as many points to the left of the interface as to the right and this is reversed for Figure 5b. The symbols represent the computed solutions and the solid lines represent the exact solutions.

A study of discrete L_2 errors for the system computations is shown in Tables I through III. Clearly, the error is spectral for all three situations. In fact, for an equal number of mesh points on either side of the interface, the error decay is exponential. For the problem of propagating pulses, where the features needing higher resolution are continually moving, it is not surprising that the best errors are obtained when there are an equal number of mesh points on both sides of the interface.

C. Quasi-One-dimensional Nozzle Flow

One potential point of concern in using the interface approximation given by Eq. (14) regards the stability of cases where one of the eigenvalues of the coefficient matrix is much larger than any other. Such a situation occurs at sonic points in an ideal gas flow where one of the characteristic speeds actually vanishes.

To test this situation the nonlinear problem of steady gas flow in a quasi-one-dimensional converging-diverging nozzle was solved with the multidomain method where an interface was placed at the sonic point. The quasilinear form of the Euler gas dynamics equations for time-dependent flow in a quasi-one-dimensional nozzle without shocks can be written as

$$\begin{bmatrix} P \\ u \end{bmatrix}_t + \begin{bmatrix} u & \gamma \\ a^2/\gamma & u \end{bmatrix} \begin{bmatrix} P \\ u \end{bmatrix}_x = \begin{bmatrix} \gamma u A_x(x)/A(x) \\ 0 \end{bmatrix} \quad (22)$$

where P is the logarithm of the pressure, u is the gas velocity, γ is the ratio of specific heats, and a is the sound speed. The coefficient matrix has eigenvalues of $u + a$ and $u - a$ so that one of them is zero at a sonic point. The steady flow is found as the large time limit of the unsteady flow described by (22).

The nozzle area is given by $A(x) = x/2 + 1/x$ so the throat occurs at $x = \sqrt{2}$. For the cases run, a subsonic inflow boundary was placed at $x = 0.2$ and characteristic boundary conditions were used. After the gas accelerates through the sonic value at the throat, it leaves the nozzle supersonically so no boundary conditions are applied at the outflow.

For the gas dynamics calculations in one dimension, $\lambda^* = 1/2 (|u+a| + |u-a|)$ was chosen since this corresponds to the diagonal elements of the absolute value of the coefficient matrix. Although the problem was solved for domain interfaces in both the subsonic and supersonic portions of the nozzle, only results for a single interface at the sonic point will be shown here. (The two-dimensional example below will include a variety of interface placements.)

Figure 6 shows the steady pressure in the nozzle computed with two domains and twice as many mesh points on the right as on the left. Our tests on a variety of grids have not shown any stability difficulties in computing steady flows when placing the interface at a sonic point.

D. Two-Dimensional Transonic Flow

A more complicated problem is the two-dimensional transonic Ringleb flow. This problem allows us to study the computational efficiency of the multidomain solution algorithm as outlined in the Introduction. Kopriva, et al., [12] used this problem for a comparison of the performance of the spectral method with a second-order finite-difference method. In this section we will compare the multidomain spectral method with the single domain spectral method.

The Ringleb flow is a simple example of a two-dimensional transonic flow for which there is an exact solution. (See, for example, Courant and Friedrichs [13].) The streamlines of the physical space solution appear at large distances as parabolas which are determined from a special hodograph solution of the potential equation for steady irrotational isentropic flow. By choosing two streamlines to represent solid walls, this problem models a steady transonic flow in a duct. Figure 7 shows the Mach contours of one such duct flow.

Again we will look for the large time solution of the unsteady gas dynamics equations, this time in two dimensions. The problem in the curved duct shown in Figure 7 is mapped onto a rectangle in the stream function-potential (ψ, ϕ) coordinate system derived from the exact solution. In this

coordinate system, the unsteady equations can be written as

$$Q_t = -R \quad (23)$$

where R is the steady state residual

$$R = AQ_\phi + BQ_\psi \quad (24)$$

Since the solution is irrotational, the solution vector is chosen to be

$$Q = [P \ u \ v]^T \quad (25)$$

and the coefficient matrices are

$$A = \begin{bmatrix} U & \phi_x & \phi_y & 0 \\ a^2 \phi_x/\gamma & U & 0 & 0 \\ a^2 \phi_y/\gamma & 0 & U & 0 \\ 0 & 0 & 0 & U \end{bmatrix} \quad B = \begin{bmatrix} V & \psi_x & \psi_y & 0 \\ a^2 \psi_x/\gamma & V & 0 & 0 \\ a^2 \psi_y/\gamma & 0 & V & 0 \\ 0 & 0 & 0 & V \end{bmatrix}$$

As before, P represents the logarithm of the pressure and (u,v) represent the velocity components in the Cartesian x and y directions, respectively. The matrix coefficients are computed from the mapping derived from the exact solution and the contravariant velocity components are

$$U = u\phi_x + v\phi_y \quad \text{and} \quad V = u\psi_x + v\psi_y.$$

The physical boundary conditions for this problem represent subsonic inflow at the entrance of the duct (at the lower left of Figure 7), supersonic outflow at the exit, and the sides are treated as impermeable boundaries (walls). So that the initial boundary value problem is well-posed the boundary conditions must be chosen carefully. See Kopriva, et al., [12] for details of the procedure which follows. For the subsonic inflow, we can specify only two quantities and have chosen the total enthalpy and the angle of the flow (so $V = 0$). The quantities P and U are computed from two conditions: The first is a compatibility equation derived from the pressure equation and the normal momentum equation. The second comes from differentiating the enthalpy equation in time. From U and the condition $V = 0$, the Cartesian velocities u, v can be computed. At the outflow, no boundary conditions are needed. Finally, at the walls the normal velocity, U , must vanish. The vector Q is computed by solving the tangential momentum equation for V and a compatibility equation which combines the normal momentum and pressure equations for P .

The system of equations (22) were discretized as described above, and fourth-order Runge-Kutta was used for the time integration. For a single domain, the Chebyshev spectral grid for the Ringleb problem with 16 streamwise and 8 normal mesh intervals is shown in Figure 8. It is clear that the spectral method strongly concentrates the grid points near the walls. The largest gradients, however, occur in the streamwise direction near the sonic line (as can be seen in Figs. 7 and 9) where the streamwise mesh distribution is coarsest. These two factors contribute to the fact that the time integration step is very small and that accuracy is degraded by the lack of resolution where it is needed.

A multidomain grid distribution for which performance will be compared to the single domain method is shown in Figure 10. Six domains now cover the duct and the same number of mesh intervals as for the single domain case are used. The divisions were chosen to demonstrate the kinds of situations which the multidomain method should be able to handle. Three divisions with $6 + 5 + 5$ mesh intervals are in the streamwise direction and two are in the normal direction. With this choice, two points occur where the corners of four domains come together. The first domain boundary in the streamwise direction was chosen to appear in a subsonic region of the duct. The second domain boundary in the streamwise direction was chosen to intersect the sonic line. By dividing the normal direction into two domains, the effective mesh spacing near the walls is doubled. Finally, note that by comparing Figure 10 to Figure 7 the sonic line also intersects the domain interface in the normal direction.

To allow comparison, Figure 11 shows the Mach number contours for both the single domain and the multidomain solutions. Note particularly that the sonic line remains smooth through the domain interfaces. Table IV summarizes the performance of the single domain spectral method compared with this particular choice of grid. First, note that even with this distribution of domains, the maximum error in the pressure for the multidomain computation has not been degraded from the single grid one. In fact, the error is five percent better.

The real advantage that the splitting has had for this case, however, is that the multidomain solution relaxes more quickly to steady state for a given number of intervals and accuracy. Figure 12 compares the rate at which the discrete L_2 norm of the residual of the pressure decays for the single and multidomain cases. The results are also summarized in Table IV. From the

trend of the graph, it should take over 2 1/2 times as many iterations for the single grid residual to decay to that of the single grid residual. This is a direct result of the fact that larger time steps can be used for the multi-domain case. The choice of λ^* also affects the convergence rate: larger values up to the stability limit give faster convergence to steady state.

The advantage of a k-domain derivative computation requiring $1/k$ the amount of work as a single domain computation does not show up in this example. In fact, as Table IV indicates, the average time per iteration (time step) requires the same amount of time at 0.5 sec. on the Langley Cyber 855. This is due to the fact that there is overhead in computing the interface approximation. Doubling the number of points in each direction with the same domain distribution decreases the time per iteration for the multidomain computation to 70% of the single domain cost. Though no attempt was made to compute the interface conditions efficiently, the number of points inside each domain will have to be large compared to the number of domains for the efficiency gained by being able to use fewer points in computing derivatives to become important.

The final advantage of a multidomain method which was listed in the Introduction is that flexibility in the choice of grid point distribution is now possible. A series of calculations were made with the duct being divided into two domain intervals in each direction. As with Figure 10, the direction across the duct was divided in half and the same number of mesh points was used. In the streamwise direction, however, only one domain boundary was inserted. This boundary was inserted in several places along the duct with different numbers of points on either side.

Results of some of the computations are summarized in Table V. The division is reported in terms of the fraction of the total variation of the velocity potential along the length of the duct. The first entry in the list places the division approximately near the bend of the duct where the gradients of the solution are the highest. It is clear that with a proper choice of grid it is possible to obtain better accuracy with the multidomain distribution of a given number of grid points than with a single grid. For the best case computed here, the error is about 2 1/2 times better for the multidomain calculation.

The problem of how to properly distribute points and subdomains in general is a major one and is beyond the scope of this paper. If they are poorly placed the error can be worse than the single domain error (see Table V). For now, it is not known how to obtain the optimal point and subdomain distribution. Rather, some knowledge of the behavior of the solution must be used as a guide.

CONCLUSIONS

We have described a simple approximation which allows a multidomain spectral solution of quasilinear hyperbolic equations. Numerical examples of linear equation models and ideal gas flow show that the method gives advantages in both accuracy and efficiency over using a single domain. Dividing up a computational domain into several subdomains gives the possibility of local refinement and allows some flexibility in the distribution of mesh points. It is possible to obtain better accuracy by doing so. Also, with multiple domains it is possible to take larger time

steps than with a single domain. This increases the efficiency for using time relaxation to achieve steady state solutions.

The use of a multidomain technique is also appropriate if discontinuities are fitted as boundaries. When shocks occur within a flow, subdomains would be arranged so that each shock lies on a subdomain boundary. In smooth parts of the solution, the technique described here would be used. Along shock interfaces, a shock fitting algorithm like that described in reference [1] can be used (Kopriva and Hussaini, to be published).

The theoretical issues which remain are many. Some theory for the range of values which λ^* can take for the method to be stable must be found. However, choosing λ^* to be the average of the largest and smallest eigenvalues of the coefficient matrix has always worked. Finally, like the problems associated with the p- version of the finite-element method, the choice of domain and point distribution for a given number of points is an open issue.

ACKNOWLEDGEMENTS

The author would like to thank Dr. S. F. Davis and Professor L. N. Trefethen for helpful comments and suggestions, and the Massachusetts Institute of Technology for computer equipment used in the course of the investigation.

REFERENCES

1. M. Y. Hussaini, D. A. Kopriva, M. D. Salas, and T. A. Zang, "Spectral methods for the Euler equations: part II - Chebyshev methods and shock fitting," AIAA J., 23 (1985), 234.
2. D. Gottlieb, M. Y. Hussaini, and S. Orszag, "Theory and application of spectral methods," in Spectral Methods for Partial Differential Equations, SIAM, Philadelphia, 1984.
3. M. Y. Hussaini, M. D. Salas, and T. A. Zang, "Spectral methods for inviscid, compressible flows," in Advances in Computational Transonics, (W. G. Habashi, Ed.), Pineridge Press, 1983.
4. C. Canuto and A. Quarteroni, "Error estimates for spectral and pseudospectral approximations of hyperbolic equations," SIAM J. Numer. Anal., 19 (1982), 629.
5. M. Berger and A. T. Jameson, "Automatic adaptive grid refinement for the Euler equations," AIAA J., 23 (1985), 561.
6. S. A. Orszag, "Spectral methods for problems in complex geometries," J. Comput. Phys., 37 (1980), 70.
7. B. Metivet and Y. Morchoisne, "Multi-domain spectral technique for viscous flow calculation," in Proceedings of the 4th GAMM conference on

Numerical Methods in Fluid Mechanics, (H. Viviand, Ed.), p. 207, Vieweg, 1982.

8. Y. Morchoisne, "Inhomogeneous flow calculations by spectral methods: mono-domain and multi-domain techniques," in Spectral Methods for Partial Differential Equations, (D. Gottlieb, M. Y. Hussaini, and R. G. Voigt, Eds.), p. 181, SIAM, Philadelphia, 1984.
9. A. T. Patera, "A spectral element method for fluid dynamics: laminar flow in a channel expansion," J. Comput. Phys., 54 (1984), 468.
10. K. Z. Korczak and A. T. Patera, "An isoparametric spectral method for solution of the Navier-Stokes equations in complex geometries," J. Comput. Phys., to appear.
11. D. Gottlieb and S. Orszag, "Numerical Analysis of Spectral Methods: Theory and Application," SIAM, Philadelphia, 1977.
12. D. A. Kopriva, T. A. Zang, M. D. Salas and M. Y. Hussaini, "Pseudospectral solution of two-dimensional gas-dynamic problems" in Proceedings of the 5th GAMM Conference on Numerical Methods in Fluid Mechanics, (M. Pandolfi and R. Piva, Eds.), Vieweg, 1984.
13. R. Courant and K. O. Friedrichs, Supersonic Flow and Shock Waves, New York, Springer-Verlag, 1976.

TABLE I. L_2 errors for the solutions to Eq. (20) with equal number of points on each side of the interface.

N	Error in u	Error in v
8	1.57×10^{-2}	1.49×10^{-2}
16	4.15×10^{-6}	4.86×10^{-6}
32	1.91×10^{-9}	1.91×10^{-9}

TABLE II. L_2 errors for the solutions to Eq. (20) with more points to the right of the interface.

N_L, N_R	Error in u	Error in v
8, 16	1.22×10^{-2}	1.05×10^{-2}
12, 24	2.45×10^{-4}	2.33×10^{-4}
16, 32	3.93×10^{-6}	3.93×10^{-6}

TABLE III. L_2 errors for the solutions to Eq. (20) with more points to the left of the interface.

N_L, N_R	Error in u	Error in v
16, 8	9.80×10^{-3}	1.04×10^{-2}
24, 12	3.48×10^{-4}	2.88×10^{-4}
32, 16	1.49×10^{-6}	2.30×10^{-6}

TABLE IV. Performance comparison for single and multidomain spectral computations.

Grids: Single Domain (SD) 17×9 points
 Multidomain (MD) $(7 + 6 + 6) \times (5 + 5)$ points
 (separated by domain)

Maximum Error

SD	1.85×10^{-3}
MD	1.74×10^{-3}

Number of Steps to Reduce Residual Three Orders of Magnitude

SD	> 1500
MD	780

Average Spectral Radius

SD	0.9964
MD	0.9942

Average Time per Iteration

SD	0.50 sec.
MD	0.50 sec.

TABLE V. Effect of streamwise mesh distribution on Ringleb calculation.

Grid	Division	Maximum Error
8 + 8	0.45 + 0.55	7.8×10^{-4}
8 + 8	0.50 + 0.50	9.3×10^{-4}
16(SD)	---	1.9×10^{-3}
10 + 6	0.34 + 0.66	1.2×10^{-2}

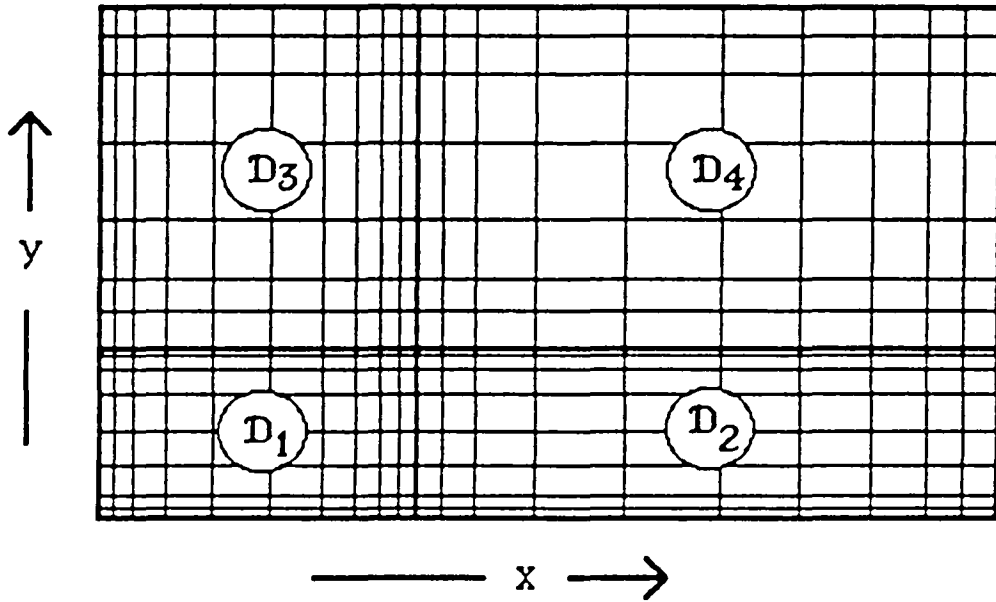


FIG. 1. Diagram of the two-dimensional subdomain structure used to divide a computational domain.

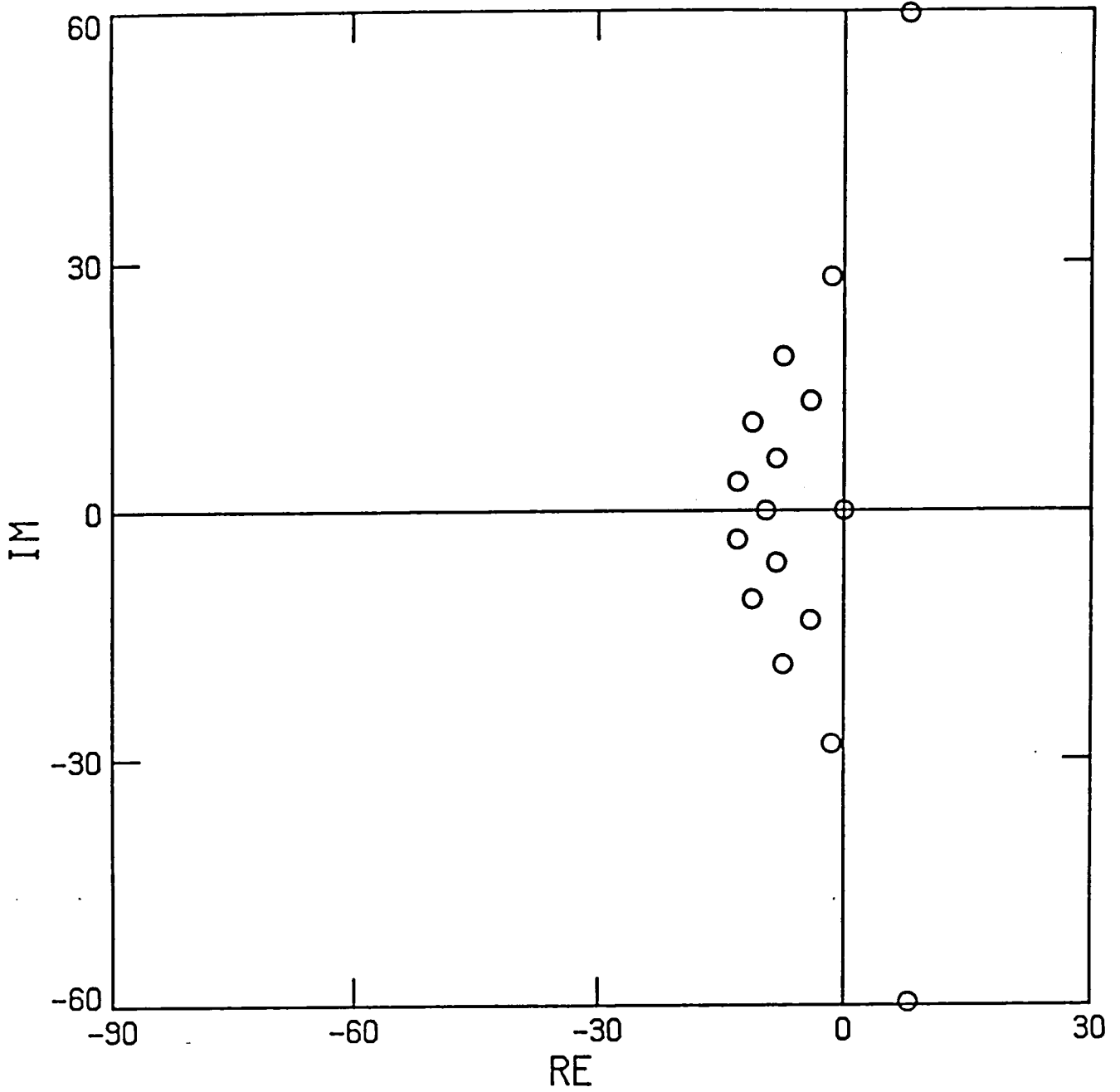


FIG. 2a. Effect on the eigenvalues of the two domain spatial approximation of the first derivative by varying λ^* in the boundary approximation:
 $\lambda^* = 0$.

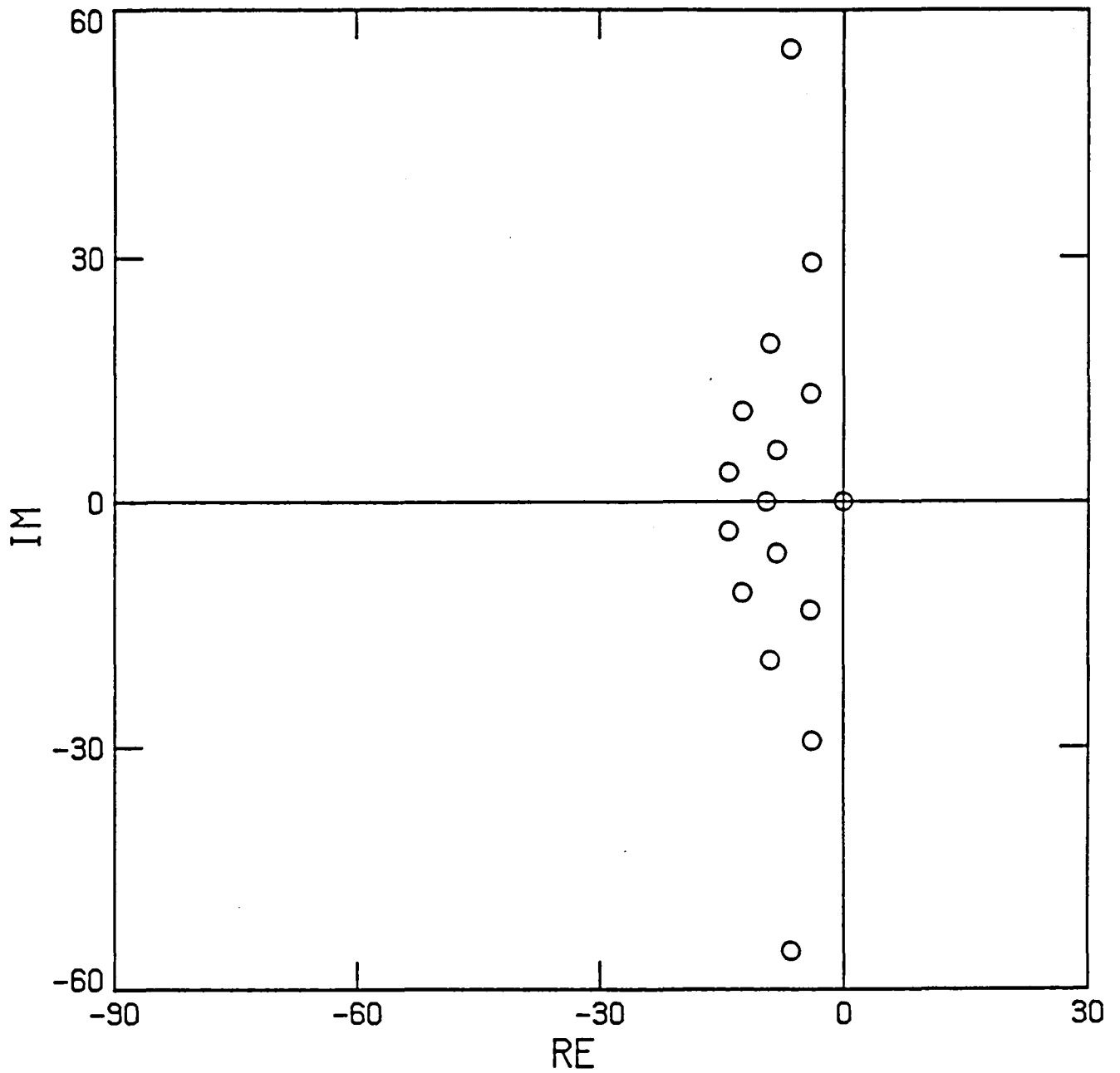


FIG. 2b. Effect on the eigenvalues of the two domain spatial approximation of the first derivative by varying λ^* in the boundary approximation: $\lambda^* = 0.5$.

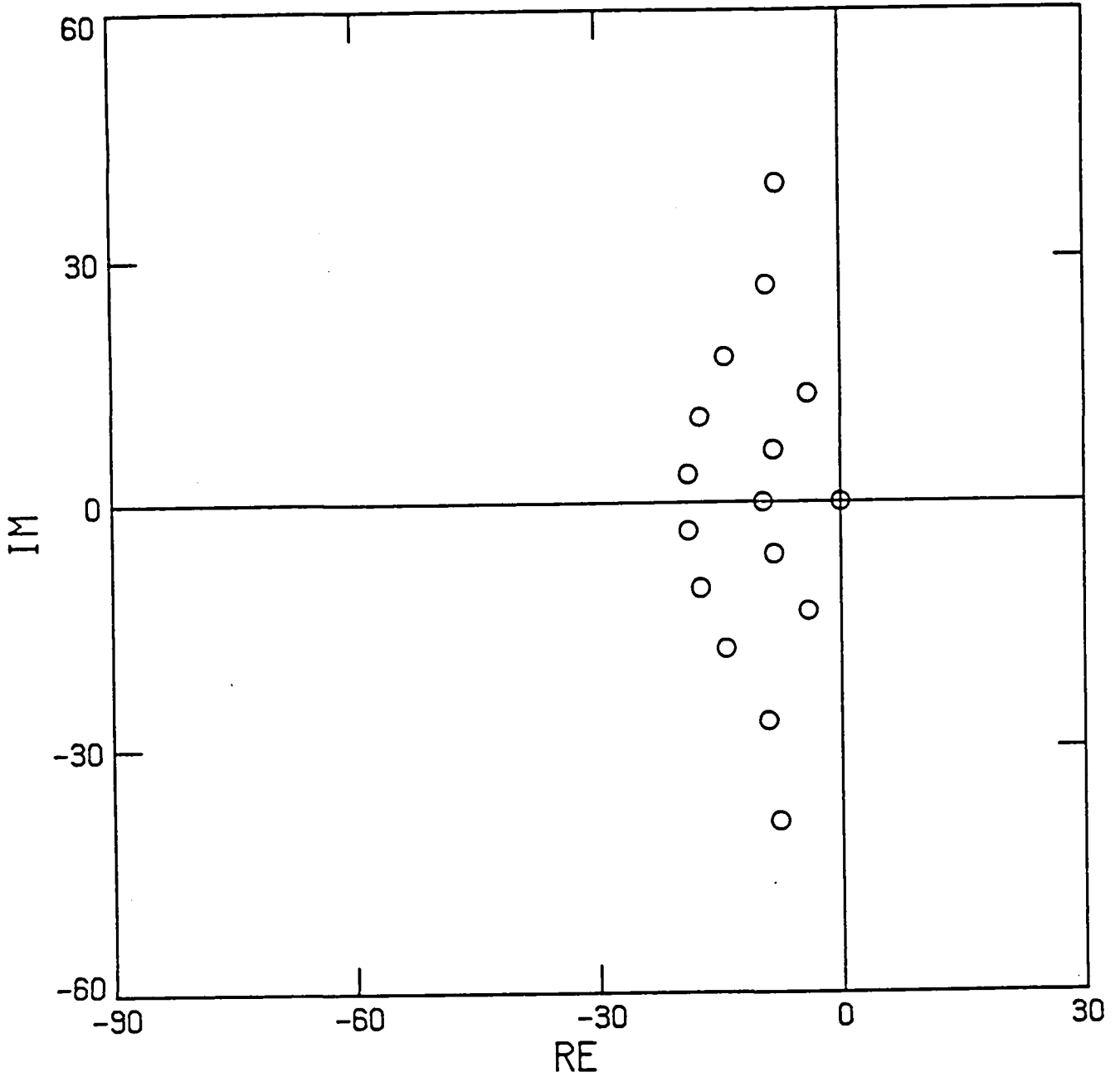


FIG. 2c. Effect on the eigenvalues of the two domain spatial approximation of the first derivative by varying λ^* in the boundary approximation: $\lambda^* = 1.0$ (purely upwind).

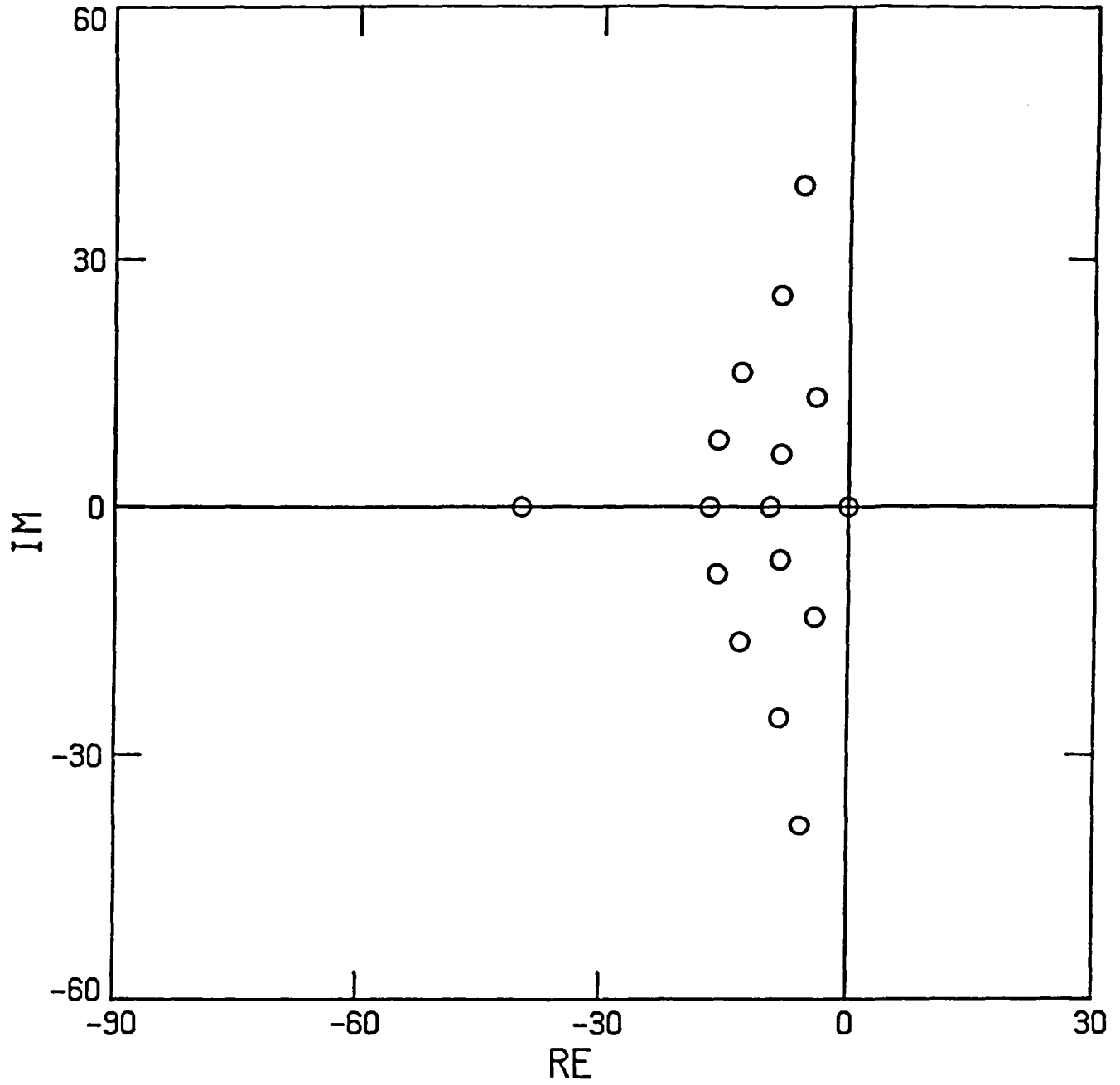


FIG. 2d. Effect on the eigenvalues of the two domain spatial approximation of the first derivative by varying λ^* in the boundary approximation: $\lambda^* = 1.1$.

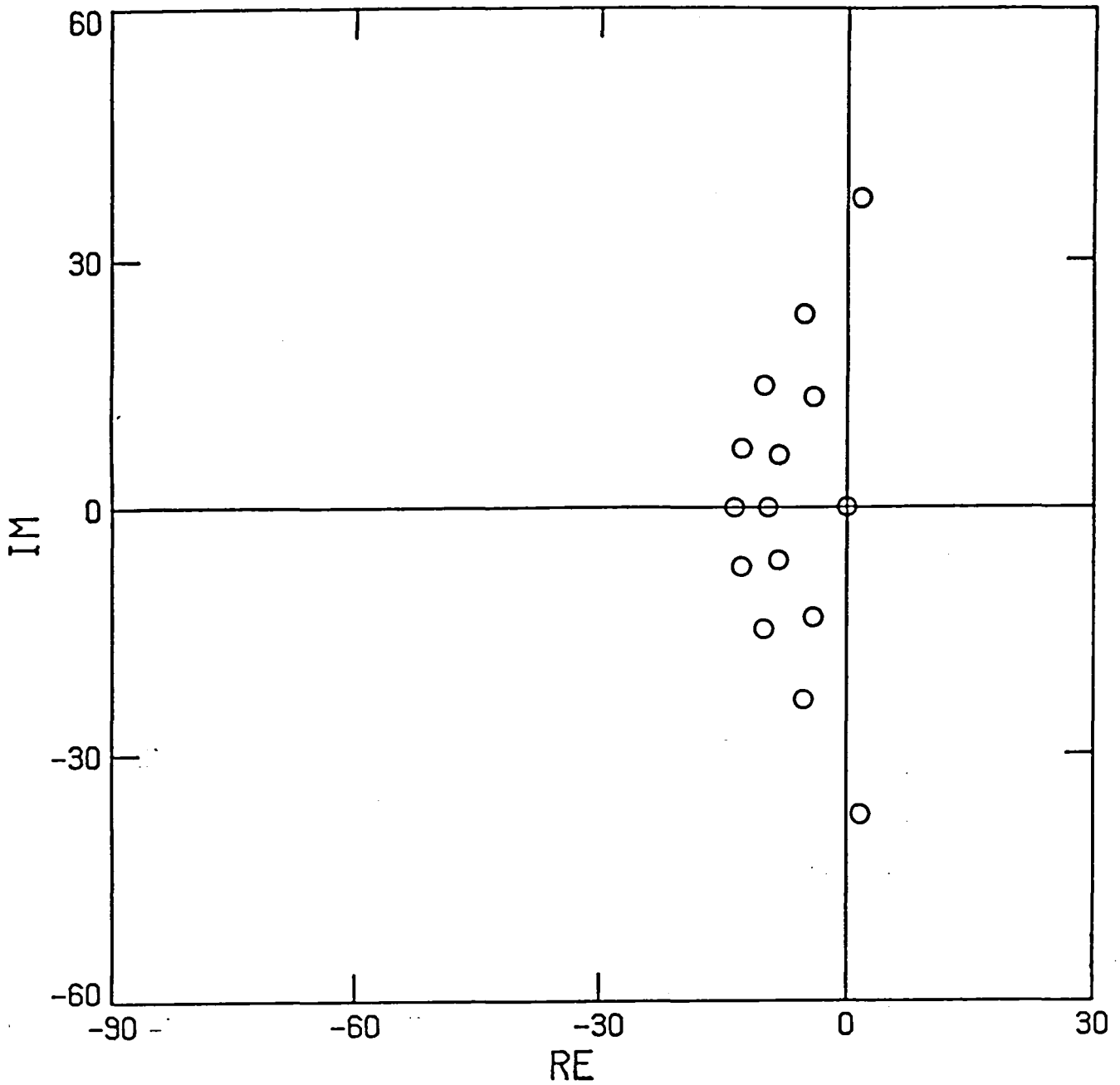


FIG. 2e. Effect on the eigenvalues of the two domain spatial approximation of the first derivative by varying λ^* in the boundary approximation:
 $\lambda^* = 5.0$.

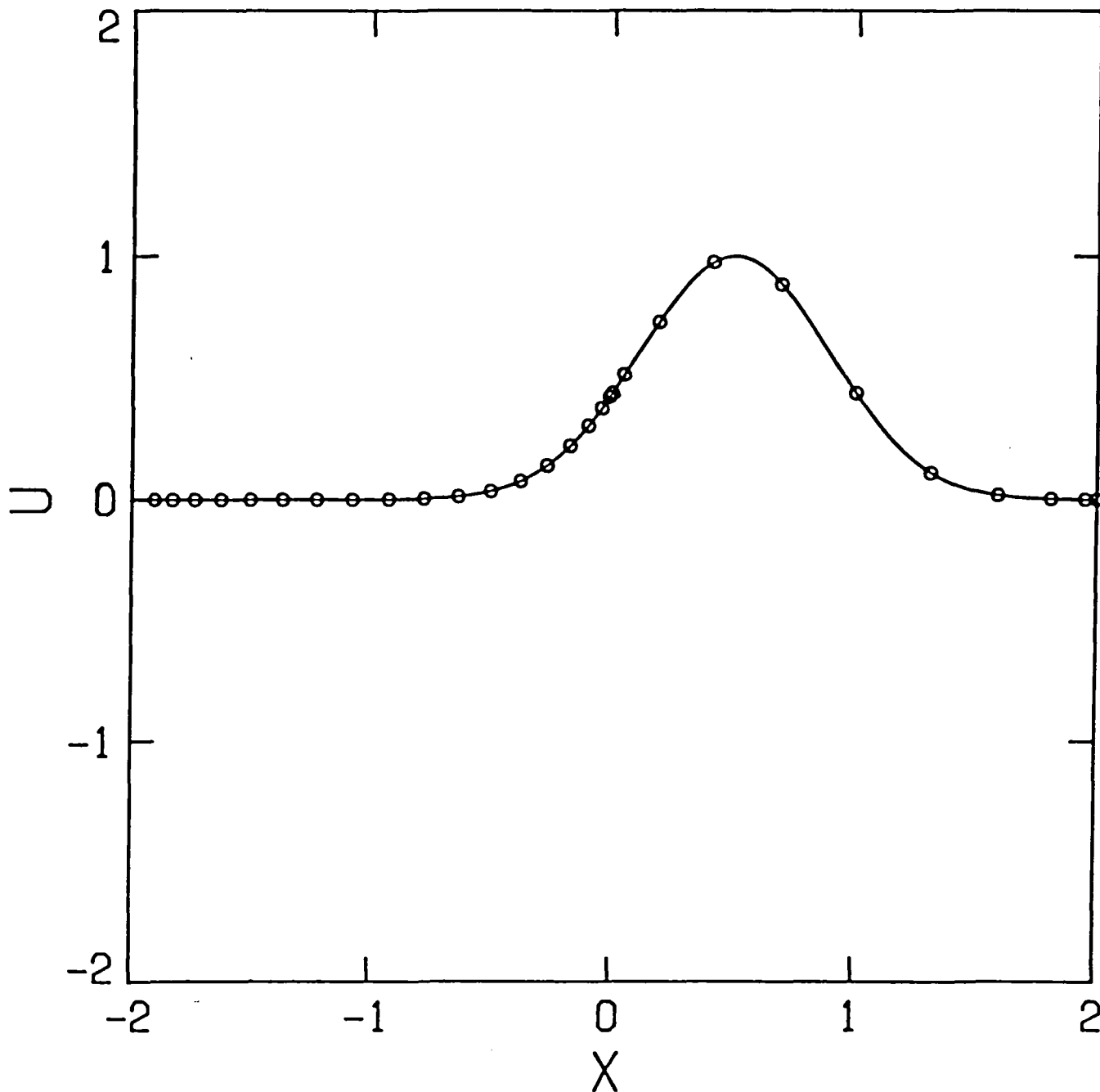


FIG. 3a. Solution of the scalar pulse problem Eq. (19) computed on two domains shown after the pulse has travelled from the left through the interface at $x = 0$. Computations are for 22 points left and 11 points right of the interface. The exact solution is the solid line; computed solutions are the circles.

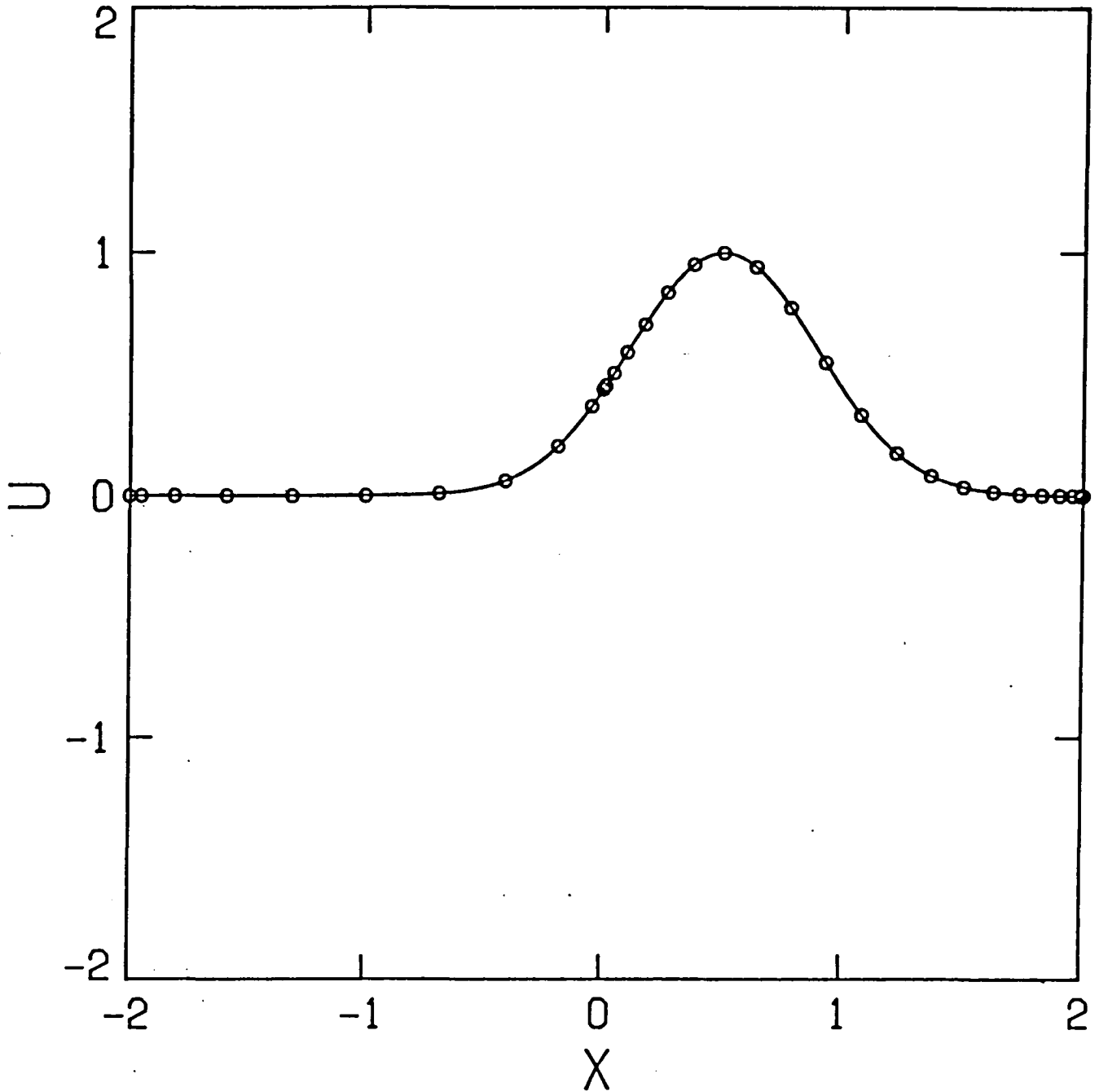


FIG. 3b. Solution of the scalar pulse problem Eq. (19) computed on two domains shown after the pulse has travelled from the left through the interface at $x = 0$. Computations are for 11 points left and 22 points right. The exact solution is the solid line; computed solutions are the circles.

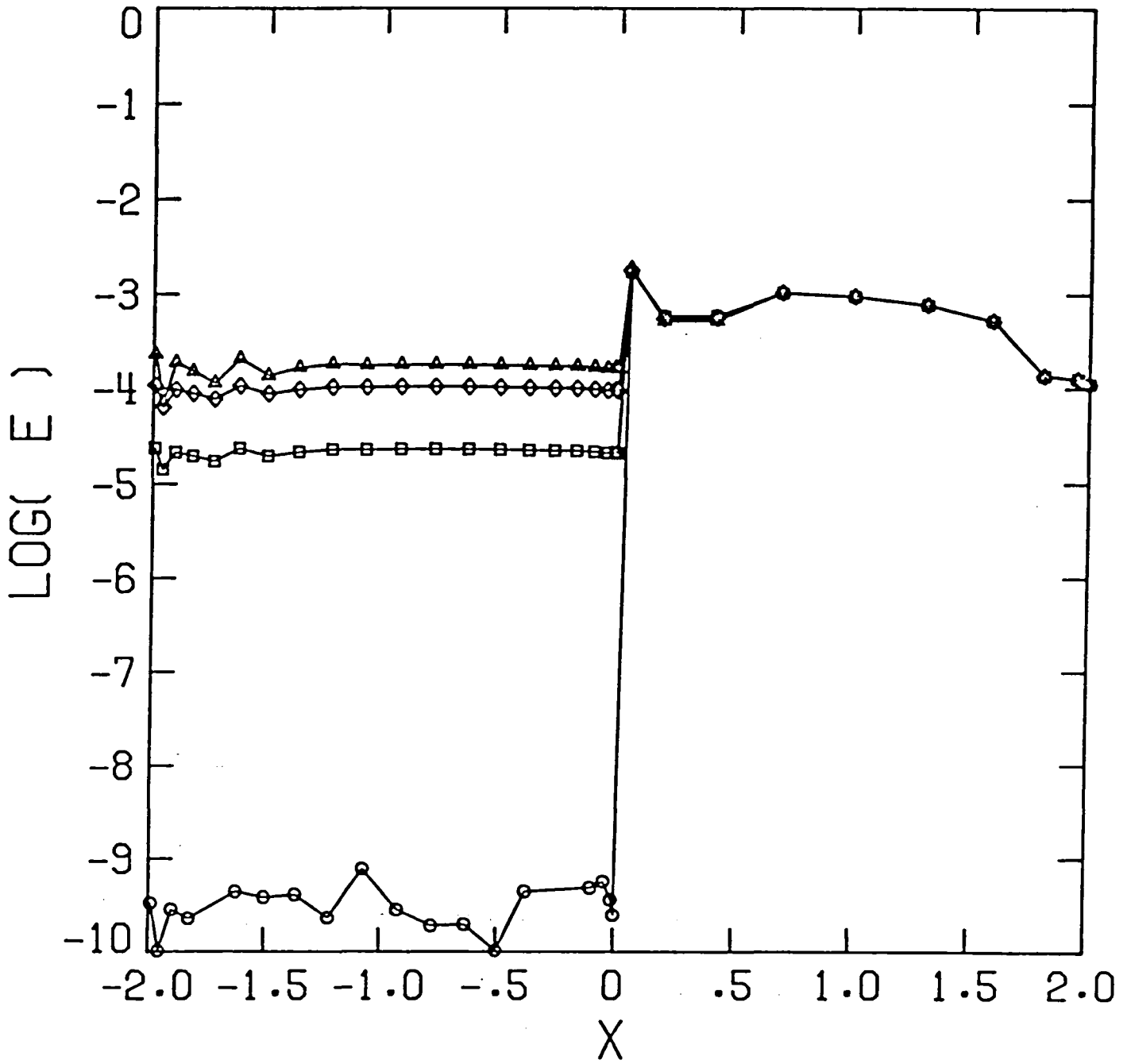


FIG. 4a. Pointwise errors as λ^* varies for the situation in Figure 3a.

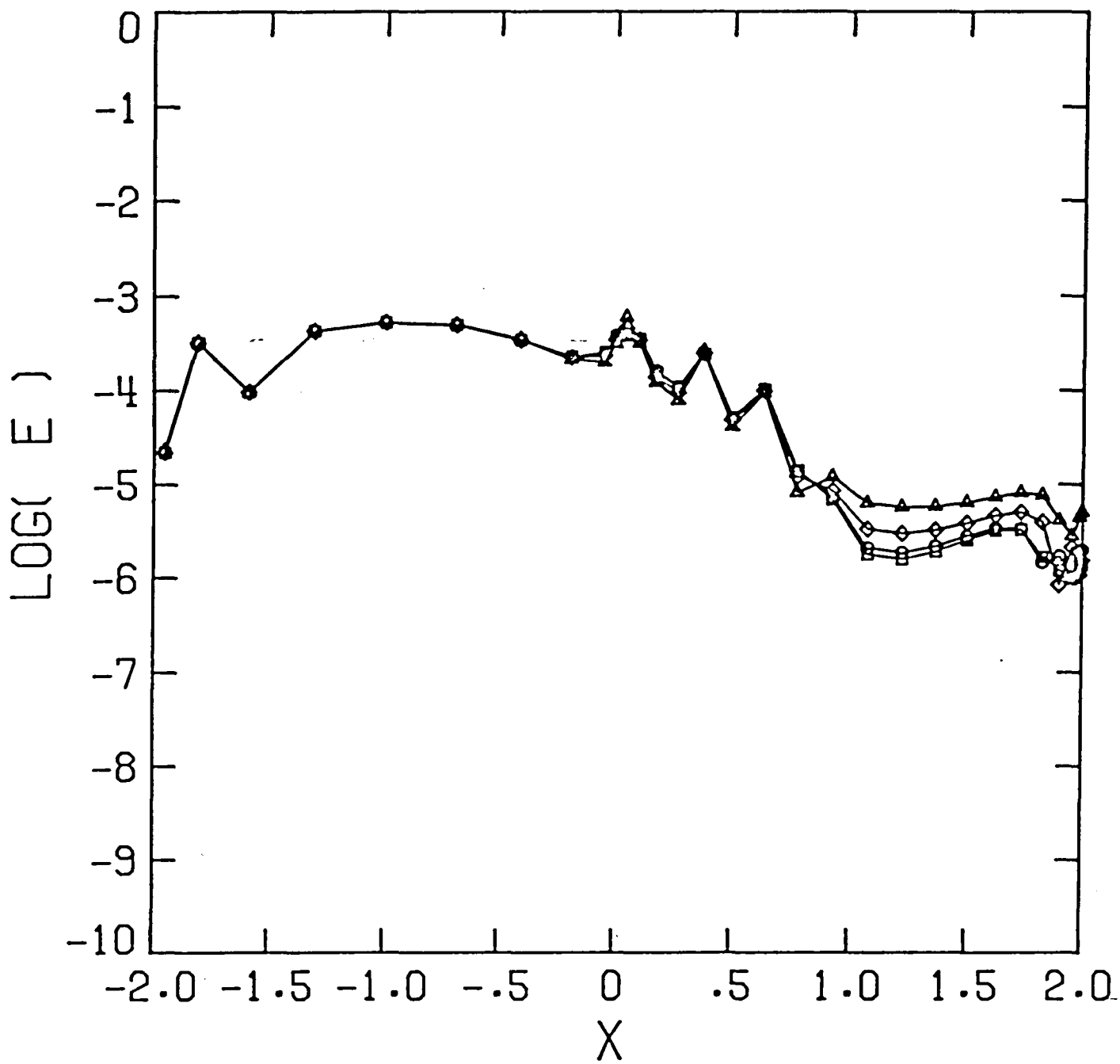


FIG. 4b. Pointwise errors as λ^* varies for the situation in Figure 3b.

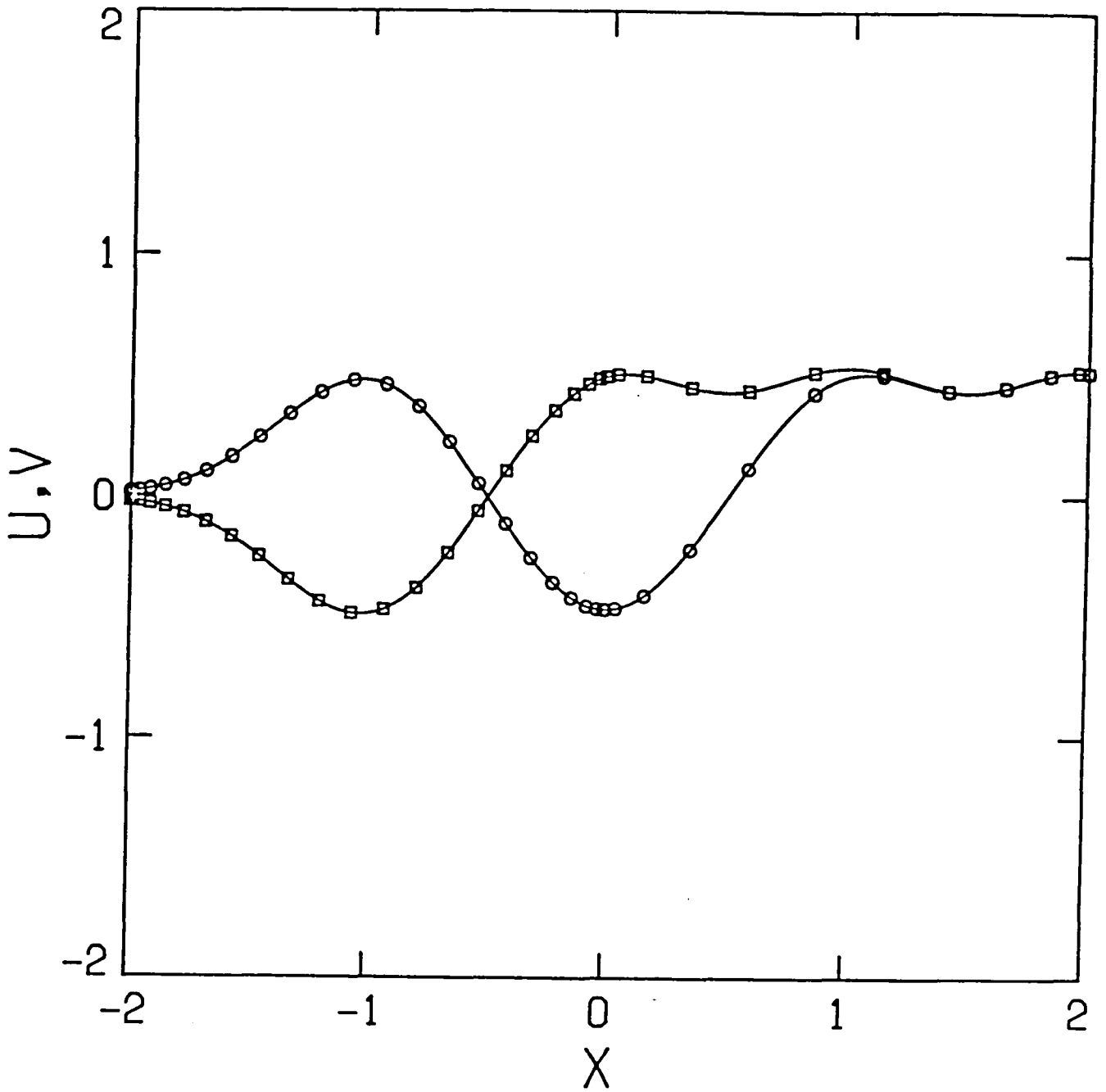


FIG. 5a. Graph of the two solutions u (circles) and v (squares) of the linear system Eq. (20) with 22 points on the left and 11 points on the right. The exact solutions are represented by the solid line.

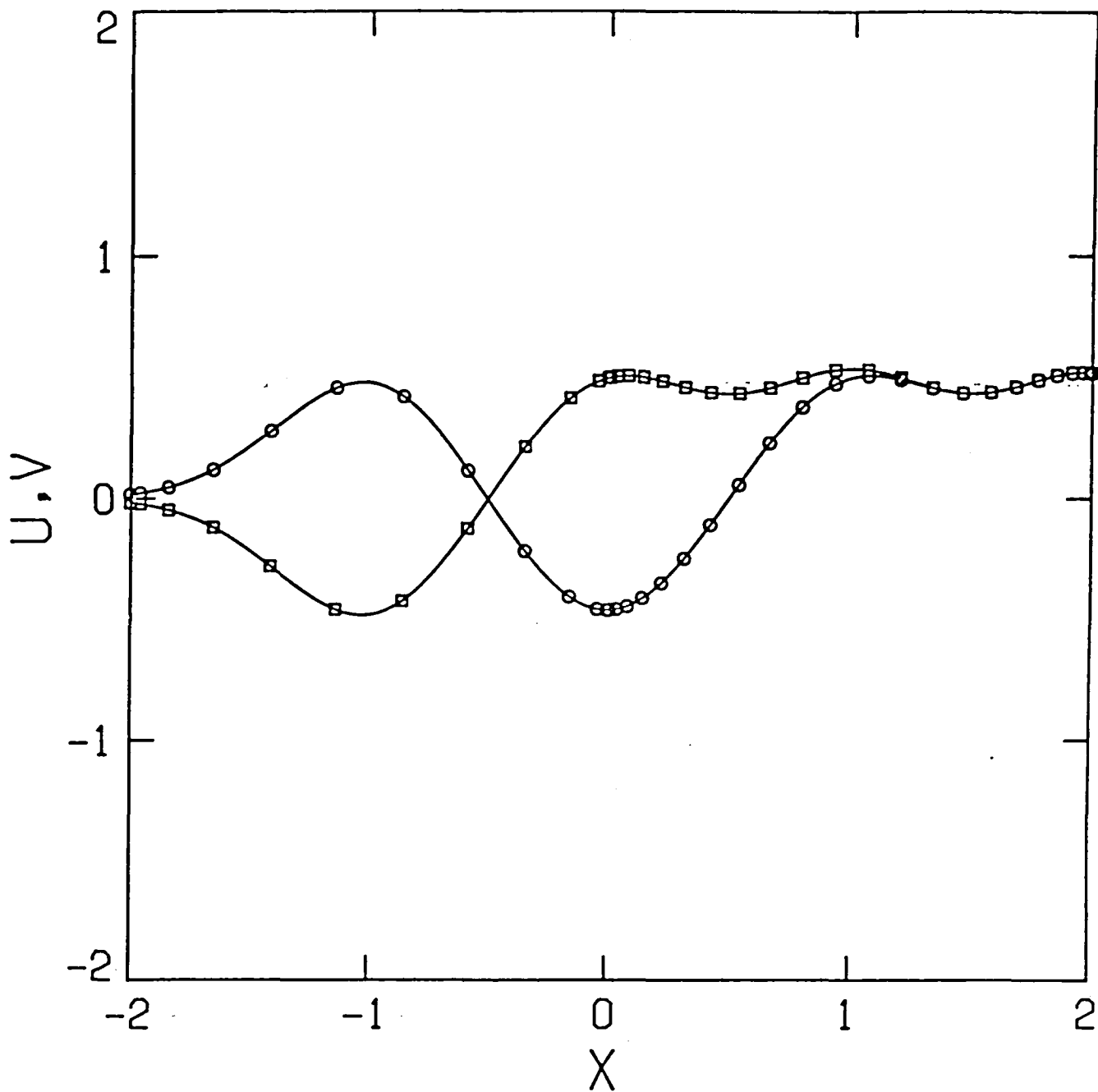


FIG. 5b. Graph of the two solutions u (circles) and v (squares) of the linear system Eq. (20) with 11 and 22 points on the left and the right. The exact solutions are represented by the solid line.

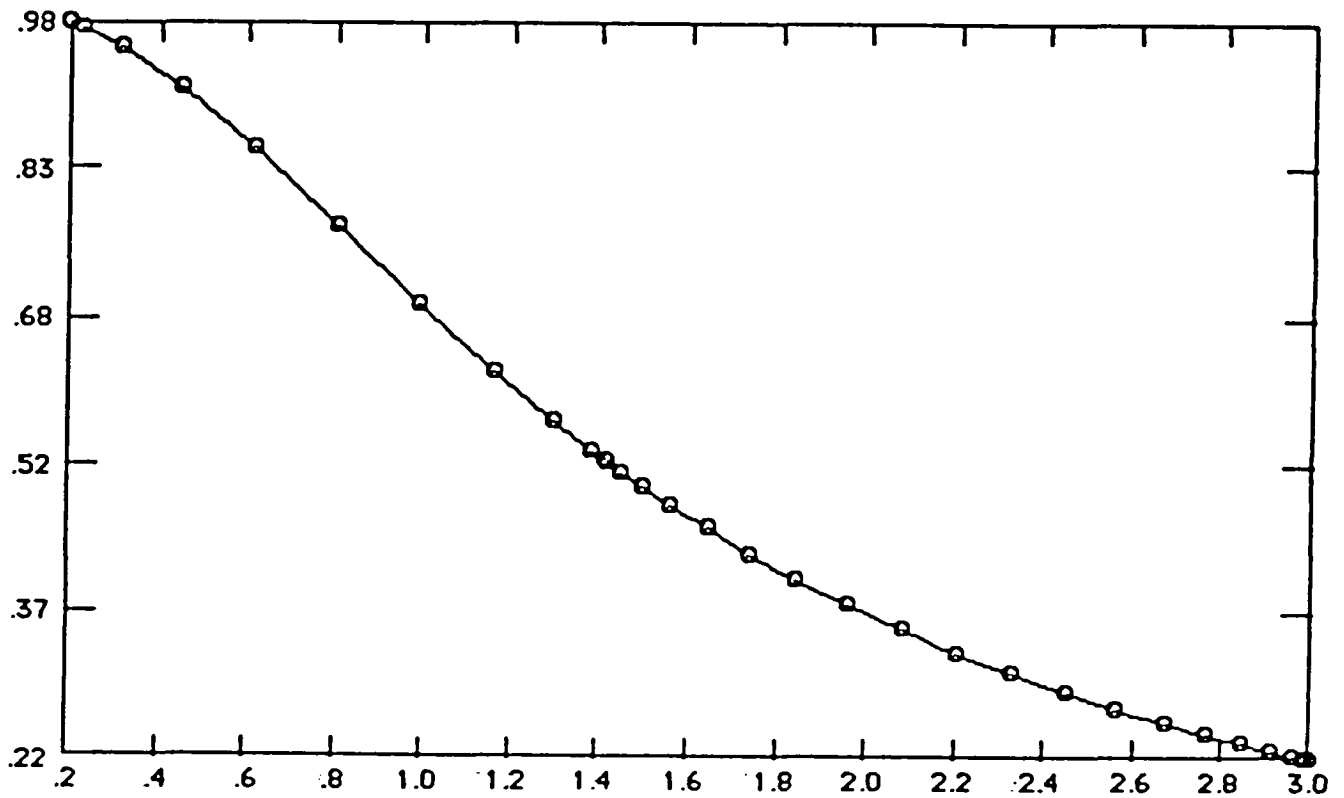


FIG. 6. Plot of the computed pressure in a converging-diverging nozzle where the interface is placed at the sonic point at $x = \sqrt{2}$. Twice as many points are used on the right as on the left of the interface.

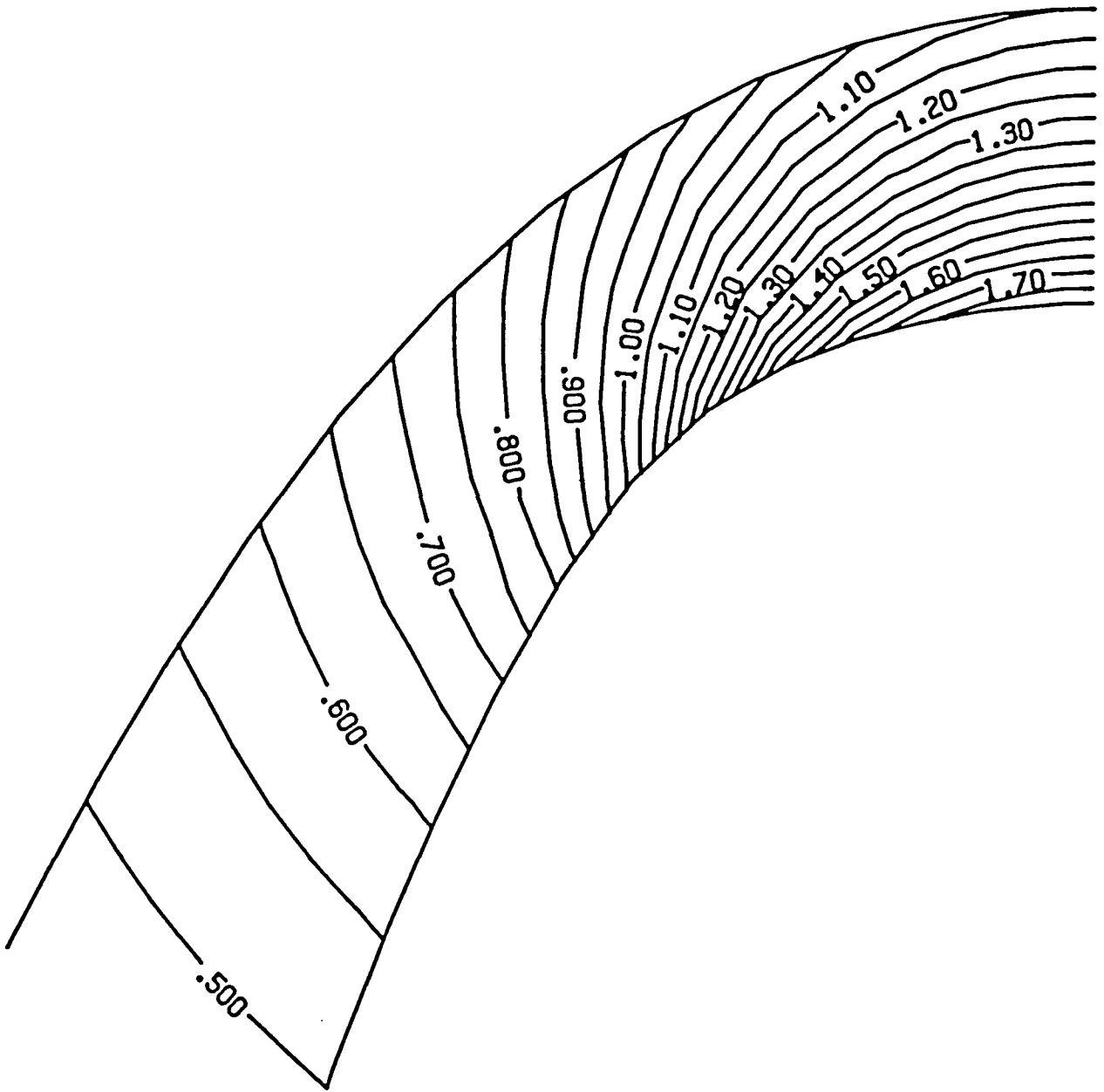


FIG. 7. Mach contours of the exact solution to the Ringleb problem which models transonic flow in a two-dimensional duct.

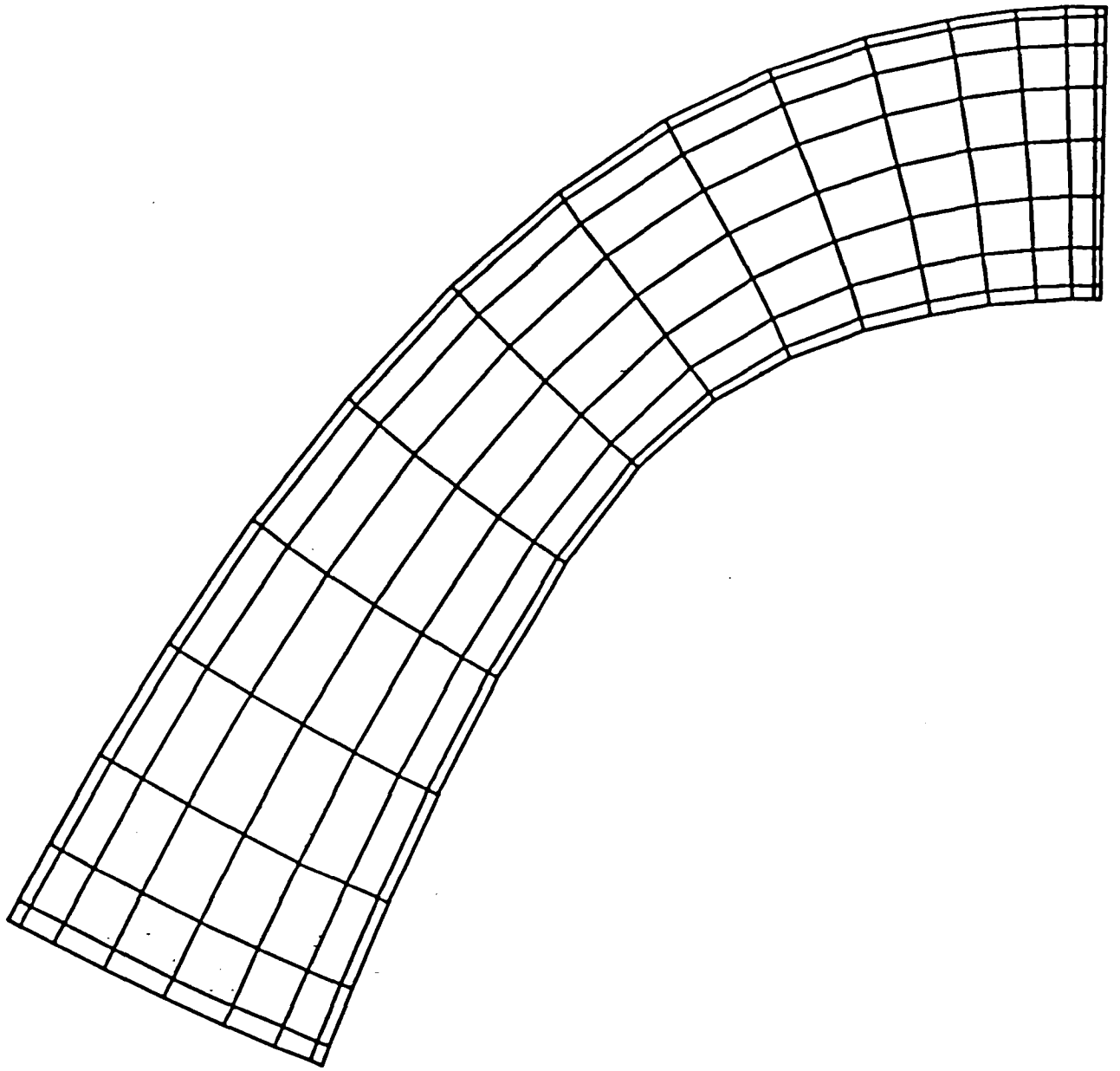


FIG. 8. Single domain Chebyshev grid for the Ringleb problem.

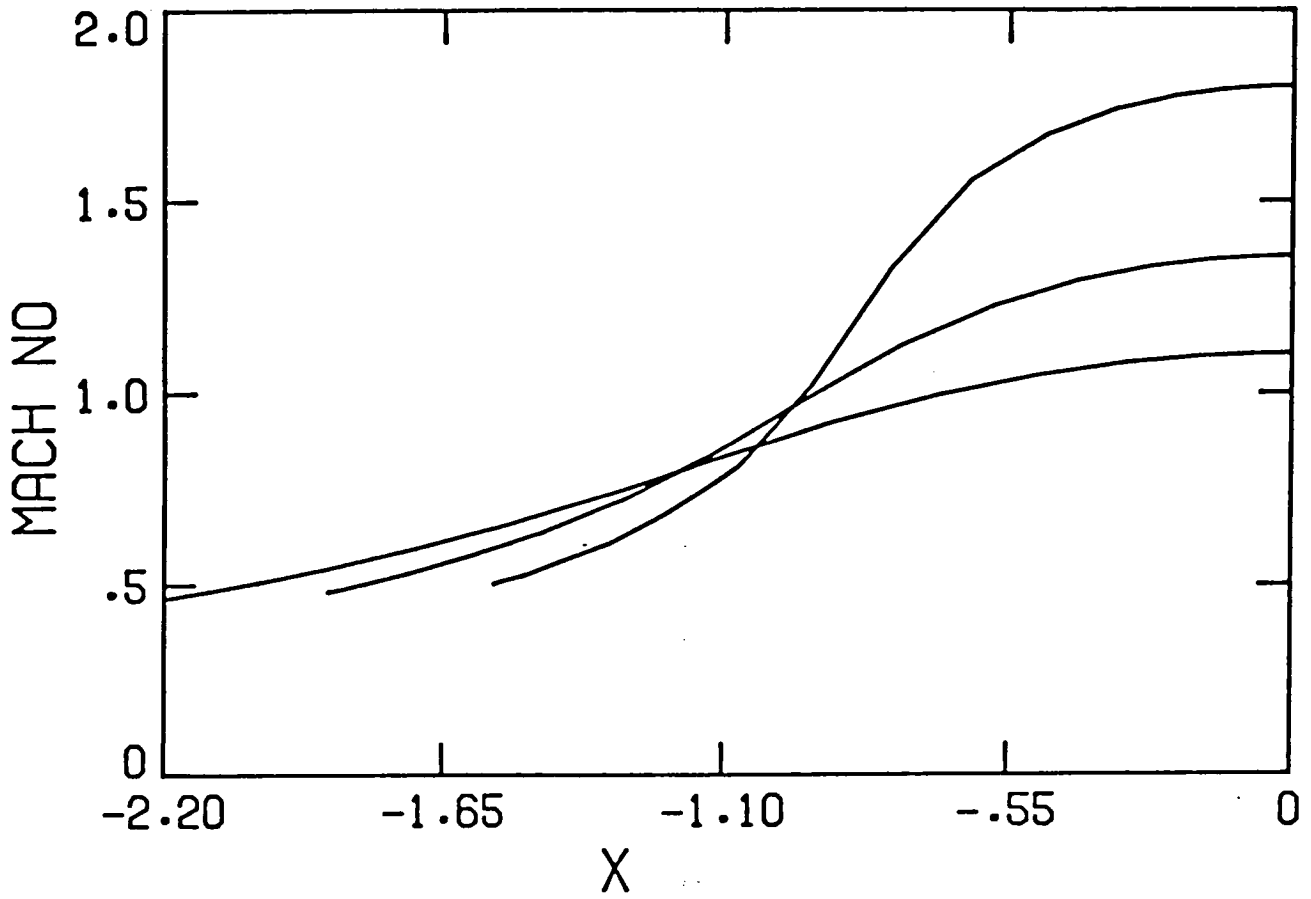


FIG. 9. Mach number variation along the lower wall, center streamline and upper wall for the Ringleb problem.

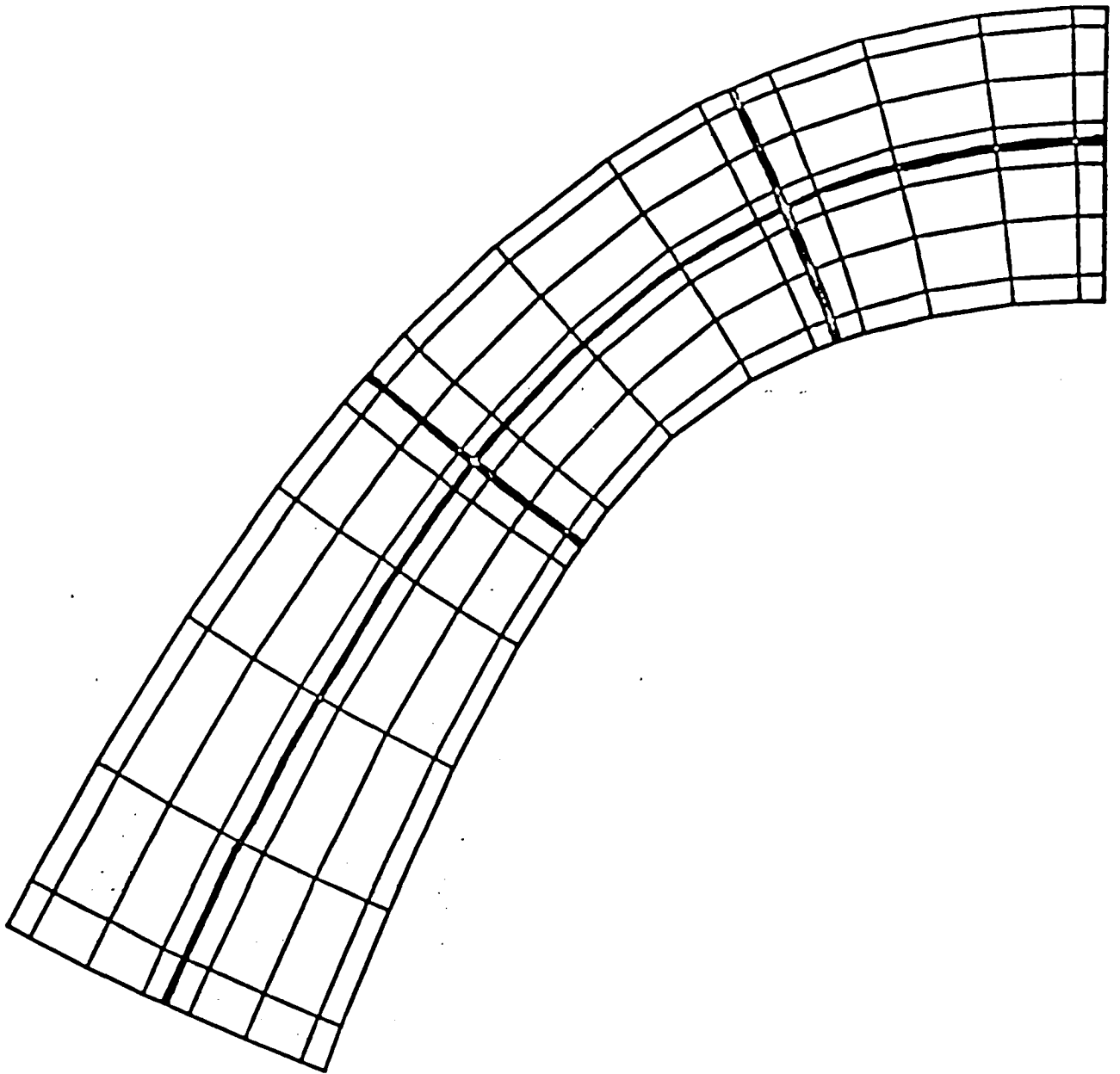


FIG. 10. Multidomain grid with six subdomains for the Ringleb problem.

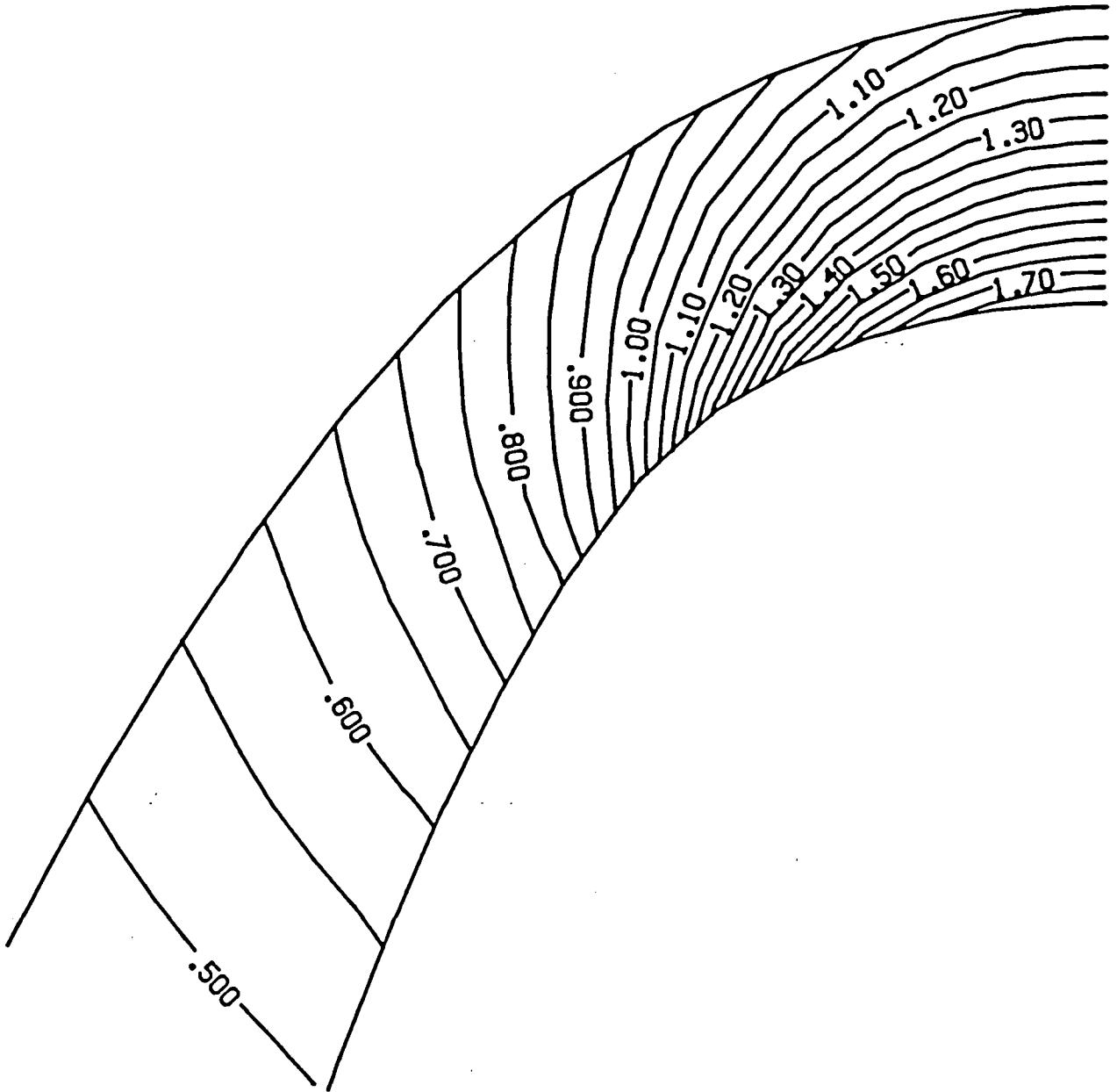


FIG. 11a. Mach number contours for single domain solution.

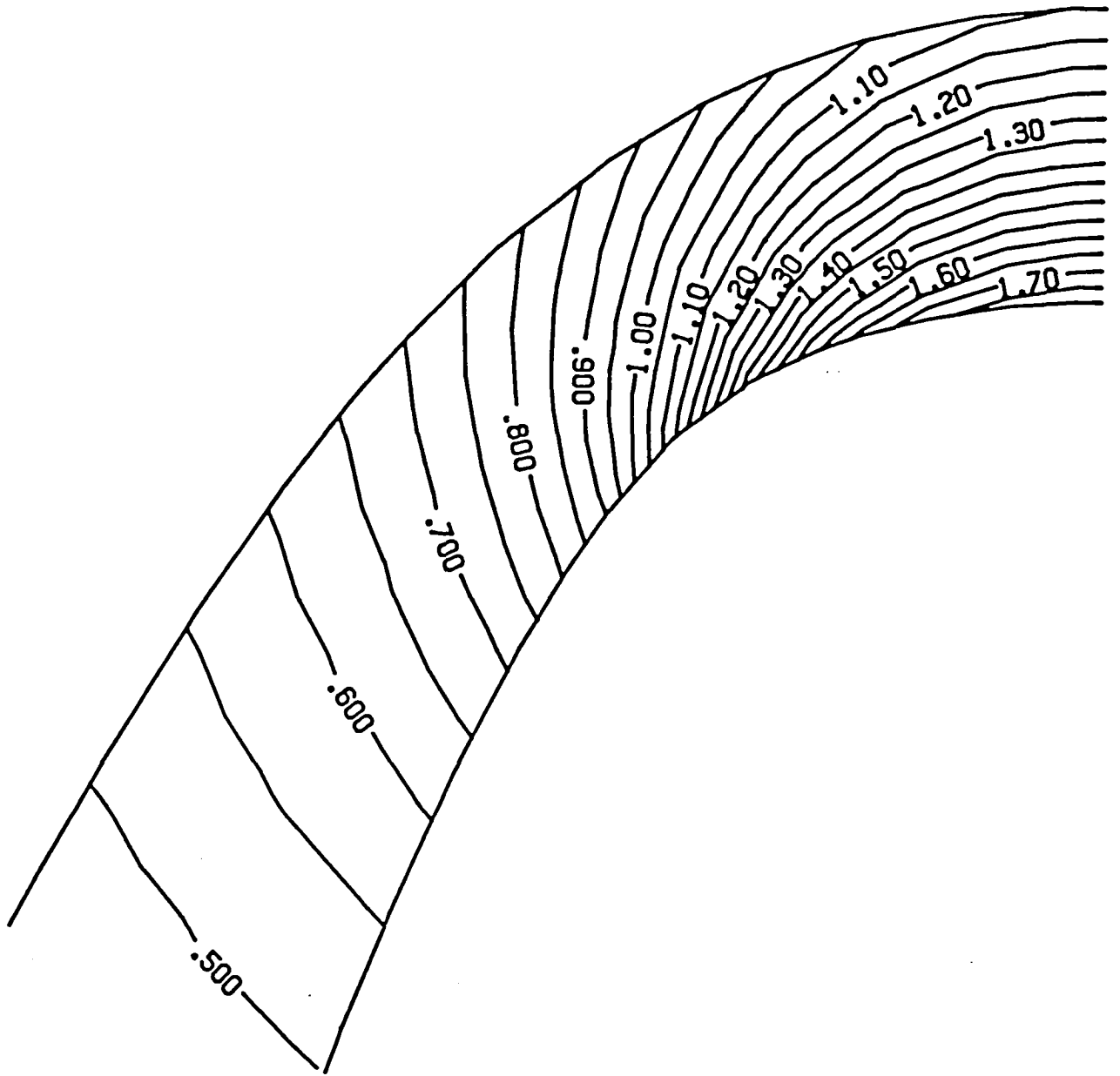


FIG. 11b. Mach number contours for six domain solution.

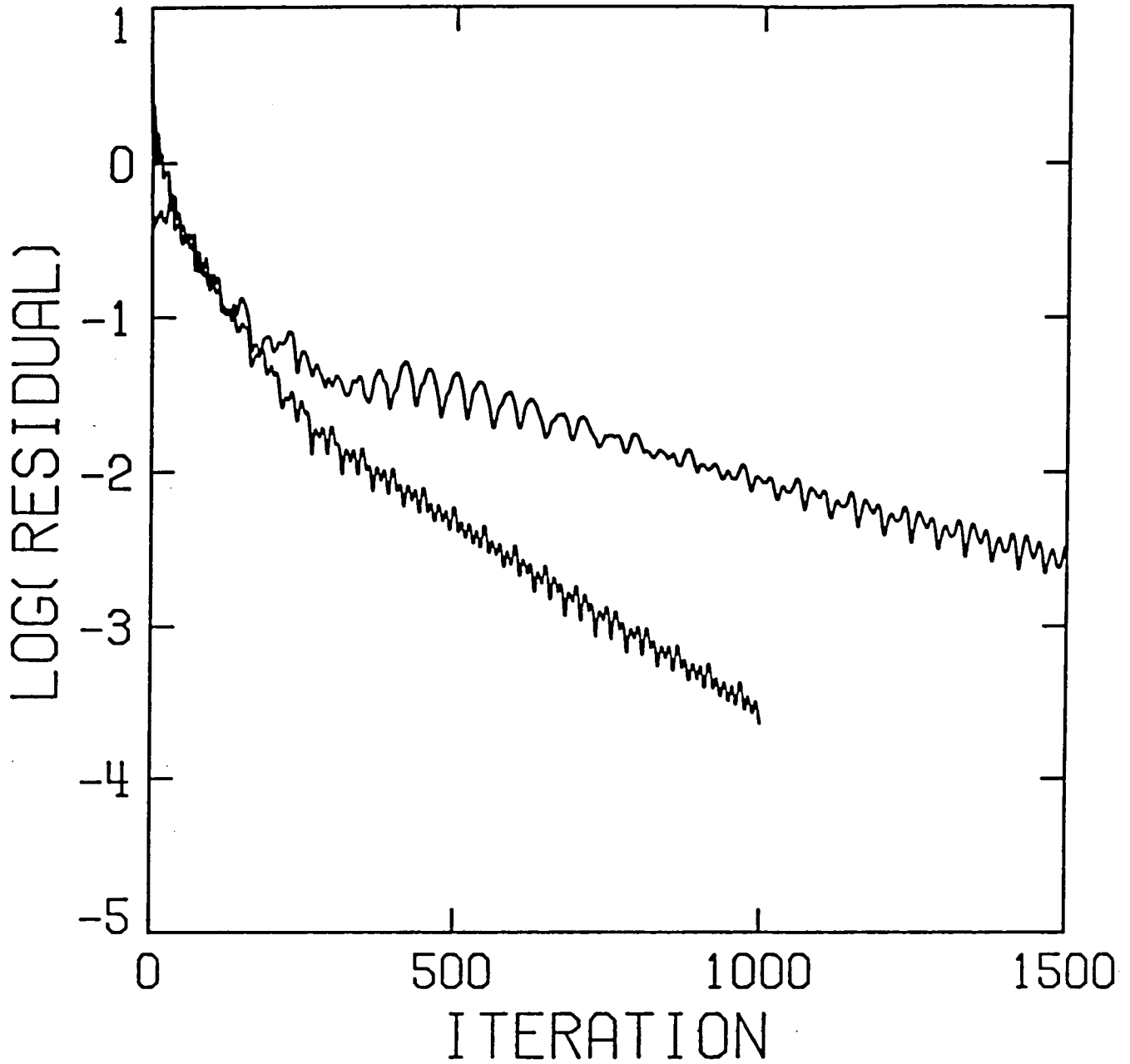


FIG. 12. Comparison of residual decay for single domain and multidomain solutions to the Ringleb problem.

1. Report No. NASA CR-178105 ICASE Report No. 86-28		2. Government Accession No.		3. Recipient's Catalog No.	
4. Title and Subtitle A SPECTRAL MULTIDOMAIN METHOD FOR THE SOLUTION OF HYPERBOLIC SYSTEMS				5. Report Date May 1986	
				6. Performing Organization Code	
7. Author(s) David Kopriva				8. Performing Organization Report No. 86-28	
				10. Work Unit No.	
9. Performing Organization Name and Address Institute for Computer Applications in Science and Engineering Mail Stop 132C, NASA Langley Research Center Hampton, VA 23665-5225				11. Contract or Grant No. NAS1-17070, NAS1-18107	
				13. Type of Report and Period Covered Contractor Report	
12. Sponsoring Agency Name and Address National Aeronautics and Space Administration Washington, D.C. 20546				14. Sponsoring Agency Code 505-31-83-01	
				15. Supplementary Notes	
Langley Technical Monitor: J. C. South				Submitted to Applied Numerical Mathematics	
Final Report					
16. Abstract A multidomain Chebyshev spectral collocation method for solving hyperbolic partial differential equations has been developed. Though spectral methods are global methods, an attractive idea is to break a computational domain into several subdomains, and a way to handle the interfaces is described. The multidomain approach offers advantages over the use of a single Chebyshev grid. It allows complex geometries to be covered, and local refinement can be used to resolve important features. For steady-state problems it reduces the stiffness associated with the use of explicit time integration as a relaxation scheme. Furthermore, the proposed method remains spectrally accurate. Results showing performance of the method on one-dimensional linear models and one- and two-dimensional nonlinear gas-dynamics problems are presented.					
17. Key Words (Suggested by Authors(s)) spectral methods, hyperbolic equations, gas-dynamics			18. Distribution Statement 64 - Numerical Analysis Unclassified - unlimited		
19. Security Classif.(of this report) Unclassified		20. Security Classif.(of this page) Unclassified		21. No. of Pages 47	22. Price A03

